

## CHAPTER 2

# RELIABILITY MODELS FOR COMBINATIONS OF EXTREME EVENTS

This chapter describes the models used to perform the reliability analysis of bridges subjected to extreme load events and their combinations. The chapter is divided into six sections. Section 2.1 presents the design nominal loads as specified in the current AASHTO LRFD and reviews the current code's methods for combining the effects of the extreme load events of interest to this study. Section 2.2 gives a brief review of the concepts of structural reliability theory and its application for calibration of structural design codes. Section 2.3 describes the resistance models used for member and system capacity. Section 2.4 describes the reliability models for the pertinent individual loads. Section 2.5 describes the risk analysis model used for the combination of loads. Section 2.6 concludes the chapter.

### 2.1 LOADS AND RETURN PERIODS IN AASHTO LRFD

The specification of load combinations in structural design codes includes the required nominal (i.e., design) loads or return periods as well as their corresponding load factors. Figure 2.1 shows the table of load factors given in the current AASHTO LRFD (Table 3.4.1). Nominal loads are usually associated with some long-term historical event that defines the loading. For example, the bridge design specifications require the design for the 50-year wind, the 2,500-year earthquake, the 75-year maximum live load, and the 100-year flood for scour. The load factors used are normally equal to or greater than 1.0 when each load is analyzed individually. When the load factor is greater than 1.0, it means that the true return period for the design event is greater than the specified nominal return period. This section reviews the current AASHTO nominal design loads and return periods for the loads of interest to this study.

#### 2.1.1 Dead Load

The LRFD code uses a set of dead load factors that reflect the differences in the levels of uncertainties associated with estimating the weight of cast-in-place elements (particularly wearing surfaces) to those of pre-cast elements. Following common practice, the nominal (design) dead load is the best estimate obtained from design plans for new bridges or from inspection of existing bridges.

#### 2.1.2 Live Load

Nowak (1999) calibrated the nominal HL-93 design truck loading model to match a projected expected 75-year maximum live load effect for all span ranges. The 75-year load projection was obtained based on truck weight data collected in the province of Ontario assuming a heavy volume (about 5,000 trucks per day) of truck traffic. The HL-93 load model was developed to represent the effects of live loads on short- to medium-span bridges for two-lane traffic. Multipresence factors are used to account for the differences between the HL-93 truck load effect and the expected maximum 75-year load for bridges with one lane or three or more lanes. Although the HL-93 load effects are slightly lower than the calculated maximum 75-year load effects, it is noted that the Ontario data used to calibrate the HL-93 load model contains a large level of conservativeness because it is biased toward the heavily loaded trucks. Similarly, the number of side-by-side events used to account for multiple-occurrence probabilities is also highly conservative. Moses (2001) gives a more complete discussion of these factors.

The HL-93 loading consists of a truck with similar configuration and axle weights as the HS-20 truck used in the AASHTO standard specifications (AASHTO, 1996). The truck has axle weights of 35 kN, 145 kN, and 145 kN (8, 32, and 32 Kips) along with axle spacing of 4.3 m (14 ft) and 4.3 to 9.0 m (14 to 30 ft). In addition, the HL-93 model stipulates that a lane load of 9.3 N/mm (0.64 kip/ft) should be used. For continuous bridges, two trucks are used (one in each span) along with the lane load. However, a reduction factor equal to 0.90 is included for multispan bridges. The dynamic factor of 1.33 is applied to the truck load alone excluding the effect of the lane load.

#### 2.1.3 Earthquake Load

The design earthquake intensities specified in the current AASHTO LRFD are based on a 475-year return period for essential bridges and 2,500-year return period for critical bridges. Maps giving the design peak ground accelerations for different regions of the United States are provided by AASHTO (Figure 3.10.2; AASHTO, 1998) based on the work of NEHRP (NEHRP, 1997). The specified load factor is 1.0. The basis of the design is the inelastic response of bridges

LOAD COMBINATION	DC	LL	WA	WS	WL	FR	TU	TG	SE	EQ	IC	CT	CV
	DD	IM					CR						
	DW	CE					SH						
	EH	BR											
LIMIT STATE	EV	PL											
	ES	LS											
Strength I	$\gamma_P$	1.75	1.00	–	–	1.00	0.50/ 1.20	$\gamma_{TG}$	$\gamma_{SE}$	–	–	–	–
Strength II	$\gamma_P$	1.35	1.00	–	–	1.00	0.50/ 1.20	$\gamma_{TG}$	$\gamma_{SE}$	–	–	–	–
Strength III	$\gamma_P$	–	1.00	1.40	–	1.00	0.50/ 1.20	$\gamma_{TG}$	$\gamma_{SE}$	–	–	–	–
Strength IV EH, EV, ES, DW, DC ONLY	$\gamma_P$ 1.5	–	1.00	–	–	1.00	0.50/ 1.20	–	–	–	–	–	–
Strength V	$\gamma_P$	1.35	1.00	0.40	0.40	1.00	0.50/ 1.20	$\gamma_{TG}$	$\gamma_{SE}$	–	–	–	–
Extreme Event I	$\gamma_P$	$\gamma_{EQ}$	1.00	–	–	1.00	–	–	–	1.00	–	–	–
Extreme Event II	$\gamma_P$	0.50	1.00	–	–	1.00	–	–	–	–	1.00	1.00	1.00
Service I	1.00	1.00	1.00	0.30	0.30	1.00	1.00/ 1.20	$\gamma_{TG}$	$\gamma_{SE}$	–	–	–	–
Service II	1.00	1.30	1.00	–	–	1.00	1.00/ 1.20	–	–	–	–	–	–
Service III	1.00	0.80	1.00	–	–	1.00	1.00/ 1.20	$\gamma_{TG}$	$\gamma_{SE}$	–	–	–	–
Fatigue—LL, IM and CE only	–	0.75	–	–	–	–	–	–	–	–	–	–	–

Figure 2.1. AASHTO LRFD load combination and load factor table (see Appendix A for definition of table symbols).

due to earthquakes. The inelastic behavior and the ductility capacity of bridge members are reflected through the use of the response modification factor  $R$ . Thus, material nonlinearity and system effects are indirectly taken into consideration. Also, the effect of the soil condition on the response is accounted for by using different correction factors for different types of soil. The earthquake design spectrum is given in terms of the natural frequencies of the bridge and is based on best estimates of the weight and the bridge elastic stiffness.

NCHRP Project 12-49 has proposed a comprehensive set of LRFD design specifications for the seismic design of bridges (see *NCHRP Report 472: Comprehensive Specification for the Seismic Design of Bridges* [Applied Technology Council {ATC} and the Multidisciplinary Center for Earthquake Engineering Research {MCEER}, 2002]). The proposed specifications use the NEHRP 2,500-year return period earthquake hazard maps along with the response spectra proposed by NEHRP but remove a two-thirds reduction factor that was

associated with the NEHRP spectral accelerations. The two-thirds factor had been included by NEHRP to essentially reduce the 2,500-year spectrum to an equivalent 500-year spectrum for the U.S. west-coast region.

#### 2.1.4 Wind Load

The AASHTO LRFD wind load provisions are based on the assumption that no live loads will be present on the bridge when wind velocities exceed 90 km/h (56 mph). According to the AASHTO LRFD commentaries, this assumption is based on “practical experience.” The basic wind speed used is 160 km/h (100 mph) although the option of using other values is permitted. Wind speeds may be taken from the ASCE 7-95 provisions to reflect regional and geographical effects. The ASCE 7-95 maps have a return period of 50 years. The stipulated AASHTO LRFD wind load factor of 1.4 indicates

that the effective return period is higher than 50 years. A comparison between the ASCE 7-95 wind maps and the data provided by Simiu et al. (1979) and Ellingwood et al. (1980) reveal that the maps provide a conservative upper limit envelope to the actual measured maximum 50-year winds.

The AASHTO LRFD contains methods to perform the wind analysis based on boundary layer theory combined with empirical observations. For wind on live loads, the AASHTO LRFD uses a distributed force of 1.46 N/mm (0.1 kip/ft) at 1800 mm (6 ft) above the roadway applied to the tributary areas that “produce load effects of the same kind.” The 1.46 N/mm corresponds to the 90 km/h (56 mph) wind speed that is the limiting speed at which live load would be present on the structure.

### 2.1.5 Vessel Collision

The AASHTO LRFD requirements for vessel collision are based on the probability of bridge collapse using factors related to the site, the barge size, and the geometry of the waterway. According to AASHTO LRFD, the acceptable annual frequency of collapse is 0.0001 for critical bridges and 0.001 for other bridges. AASHTO LRFD stipulates that the probability of collapse should be calculated based on the number of vessels, the probability of vessel aberrancy, the geometric probability of collision given an aberrant vessel, and the probability of bridge collapse given a collision. The AASHTO LRFD provides an empirical equation to obtain the probability of bridge collapse given that a collision has occurred. Conservative assumptions are implicitly included in many of the empirical equations used in the safety check process (e.g., estimation of barge impact force), in effect further reducing the probability of collapse. The load factor specified is set at 1.0.

### 2.1.6 Scour

The AASHTO LRFD specifications require that scour at bridge foundations be designed for the 100-year flood storm surge tide or for the overtopping flood of lesser recurrence interval. The corresponding 100-year design scour depth at bridge foundations is estimated following the procedure recommended by FHWA using the manual known as “HEC-18” (*Hydraulic Engineering Circular No. 18: Evaluating Scour at Bridges* [Richardson and Davis, 1995]). The foundation should then be designed while taking into consideration the design scour depth. This is achieved by, for example, placing the footings below the scour depth, ensuring that the lengths of piles and pile shafts extend beyond the scour depth, and verifying that the remaining soil depth after scour provides sufficient resistance against sliding failures and overturning.

The HEC-18 manual recognizes that the total scour at a highway crossing is composed of three components: (1) long-term aggradation and degradation, (2) contraction scour, and

(3) local scour. Aggradation and degradation are long-term elevation changes in the streambed of the river or waterway caused by erosion and deposition of material. Contraction scour is due to the removal of material from the bed and the banks of a channel often caused by the bridge embankments encroaching onto the main channel. Local scour involves the removal of material from around bridge piers and abutments. It is caused by an acceleration of flow around the bridge foundation that accompanies a rise in water levels that may be due to floods and other events. Both local scour and contraction scour can be either clear water or live bed. Live-bed conditions occur when there is a transport of bed material in the approach reach. Clear-water conditions occur when there is no bed material transport. Live-bed local scour is cyclic in nature because it allows the scour hole that develops during the rising stage of the water flow to refill during the falling stage. Clear-water scour is permanent because it does not allow for a refill of the hole. The focus of this report is on local live-bed scour around bridge piers that, because of its cyclical nature, is the most unpredictable type of scour.

### Summary

Each loading type considered in the AASHTO LRFD provisions is represented by a nominal load intensity (i.e., a code specified live load or a geographically varying load for a given return period) and a corresponding load factor. It is noticed that the design return periods differ considerably for each type of load event (e.g., 2,500-year for earthquakes, 75-year for live load, 50-year for wind, 100-year for scour, and 1-year for vessel collisions). The reasons for the differences in the design return periods are traditional use, providing consistency with other codes, and providing assurances to the public about the safety of bridges. One should note that these return periods are only nominal because by adjusting the load factors, one could produce a common “effective return period.” In addition, several of the “event intensity maps” provided as part of the specifications are based on biased envelopes of the actual measured data, and the degree of conservatism in each load analysis model varies from load type to load type. Therefore, actual failure rates may be significantly different than those implied by the nominal return periods. One major aim of structural reliability methods is to quantify these degrees of conservatism by obtaining more realistic and objective assessments of the safety levels implied in code-specified design procedures for each load type.

The calibration of the AASHTO LRFD specifications for the Strength I Limit State was undertaken using uniform reliability criteria. The code was calibrated based on the reliability of individual girders of multigirder bridges for the combination of dead and live loads. The specifications for the other extreme events of interest to this study were based on the work performed for other structural codes. In particular, AASHTO LRFD relies on the provisions and guidelines provided by

NEHRP for earthquakes, ASCE 7-95 for wind, AASHTO's *Guide Specification and Commentary for Vessel Collision Design of Highway Bridges* for vessel collisions (AASHTO 1991), and HEC-18 by FHWA for scour. In order to perform the reliability analysis and calibrate the load factors for combinations of extreme load events, statistical information on the rate of occurrence, the time duration, and the intensity of each extreme loading event is necessary. In addition, the uncertainties associated with design parameters other than the load intensities must be included. To remain consistent with the intent of the AASHTO LRFD specifications to provide safe bridge structures over an intended design life of 75 years, the load factors should be calibrated to provide consistent reliability levels for a 75-year return period, regardless of the return period that is used to define the design loads. Section 2.2 gives a review of basic concepts of reliability theory and describes the information required to perform a reliability-based evaluation of design codes. Sections 2.3 and 2.4 summarize the information available on the resistance and load models pertinent for this study and describe the methods used by various code-writing agencies and adapted in this study to account for the uncertainties associated with modeling the effect of these loads on the safety of typical bridge systems.

## 2.2 BASIC CONCEPTS OF STRUCTURAL RELIABILITY

The aim of the structural reliability theory is to account for the uncertainties encountered while evaluating the safety of structural systems or during the calibration of load and resistance factors for structural design codes. The uncertainties associated with predicting the load-carrying capacity of a structure, the intensities of the loads expected to be applied, and the effects of these loads may be represented by random variables. The value that a random variable can take is described by a probability distribution function. That is, a random variable may take a specific value with a certain probability, and the ensemble of these values and their probabilities are described by the distribution function. The most important characteristics of a random variable are its mean value or average and the standard deviation that gives a measure of dispersion or a measure of the uncertainty in estimating the variable. The standard deviation of a random variable  $R$  with a mean  $\bar{R}$  is defined as  $\sigma_R$ . A dimensionless measure of the uncertainty is the coefficient of variation (COV), which is the ratio of standard deviation divided by the mean value. For example, the COV of the random variable  $R$  is defined as  $V_R$  such that

$$V_R = \frac{\sigma_R}{\bar{R}}. \quad (2.1)$$

Codes often specify nominal values for the variables used in design equations. These nominal values are related to the

means through bias values. The bias is defined as the ratio of the mean to the nominal value used in design. For example, if  $R$  is the member resistance, the mean of  $R$ , namely  $\bar{R}$ , can be related to the nominal or design value  $R_n$  using a bias factor such that

$$\bar{R} = b_r R_n \quad (2.2)$$

where  $b_r$  is the resistance bias and  $R_n$  is the nominal value as specified by the design code. For example, A36 steel has a nominal design yield stress of 36 ksi (248,220 kPa), but coupon tests show an actual average value close to 40 ksi (275,800 kPa). Hence, the bias of the yield stress is 40/36 or 1.1.

In structural reliability, safety may be described as the situation in which capacity (strength, resistance, fatigue life, etc.) exceeds demand (load, moment, stress ranges, etc.). Probability of failure (i.e., probability that capacity is less than applied load effects) may be formally calculated; however, its accuracy depends upon detailed data on the probability distributions of load and resistance variables. Because such data are often not available, approximate models are often used for calculation.

Let the reserve margin of safety of a bridge component be defined as,  $Z$ , such that

$$Z = R - S \quad (2.3)$$

where  $R$  is the resistance or member capacity and  $S$  is the total load effect. Probability of failure,  $P_f$ , is the probability that the resistance  $R$  is less than or equal to the total applied load effect  $S$  or the probability that  $Z$  is less than or equal to zero. This is symbolized by the following equation:

$$P_f = Pr [R \leq S] \quad (2.4)$$

where  $Pr$  is used to symbolize the term probability. If  $R$  and  $S$  follow independent normal distributions, then

$$P_f = \Phi\left(\frac{0 - \bar{Z}}{\sigma_z}\right) = \Phi\left(-\frac{\bar{R} - \bar{S}}{\sqrt{\sigma_R^2 + \sigma_S^2}}\right) \quad (2.5)$$

where

$\Phi$  = the normal probability function that gives the probability that the normalized random variable is below a given value,

$\bar{Z}$  = the mean safety margin, and

$\sigma_z$  = the standard deviation of the safety margin.

Thus, Equation 2.5 gives the probability that  $Z$  is less than zero. The reliability index,  $\beta$ , is defined such that

$$P_f = \Phi(-\beta) \quad (2.6)$$

which for the normal distribution case gives

$$\beta = \frac{\bar{Z}}{\sigma_z} = \frac{\bar{R} - \bar{S}}{\sqrt{\sigma_R^2 + \sigma_S^2}}. \quad (2.7)$$

Thus, the reliability index,  $\beta$ , which is often used as a measure of structural safety, gives in this instance the number of standard deviations that the mean margin of safety falls on the safe side.

The reliability index,  $\beta$ , defined in Equations 2.6 and 2.7, provides an exact evaluation of risk (failure probability) if  $R$  and  $S$  follow normal distributions. Although  $\beta$  was originally developed for normal distributions, similar calculations can be made if  $R$  and  $S$  are lognormally distributed (i.e., when the logarithms of the basic variables follow normal distributions). Also, “Level II” methods have been developed to obtain the reliability index for the cases in which the basic variables are not normal. Level II methods, often referred to as FORM or first order second moment (FOSM) involve an iterative calculation to obtain an estimate to the failure probability. This is accomplished by approximating the failure equation (i.e., when  $Z = 0$ ) by a tangent multidimensional plane at the point on the failure surface closest to the mean value. More advanced techniques including second order reliability methods (SORMs) have also been developed. On the other hand, Monte Carlo simulations can be used to provide estimates of the probability of failure. Monte Carlo simulations are suitable for any random variable distribution type and failure equation. In essence, a Monte Carlo simulation creates a large number of “experiments” through the random generation of sets of resistance and load variables. Estimates of the probability of failure are obtained by comparing the number of experiments that produce failure with the total number of generated experiments. Given values of the probability of failure,  $P_f$ , the reliability index,  $\beta$ , is calculated from Equation 2.6 and is used as a measure of structural safety even for non-normal distributions. More detailed explanations of the principles discussed in this section can be found in published texts on structural reliability (e.g., Thoft-Christensen and Baker, 1982; Nowak and Collins, 2000; Melchers, 1999).

The reliability index has been used by many code-writing groups throughout the world to express structural risk.  $\beta$  in the range of 2 to 4 is usually specified for different structural applications (e.g.,  $\beta = 3.5$  was used for the calibration of the Strength I Limit State in AASHTO LRFD specifications). These values usually correspond to the failure of a single component. If there is adequate redundancy, overall system reliability indexes will be higher.

### 2.2.1 Code Calibration

Generally speaking,  $\beta$  is not used in practice for making decisions regarding the safety of a design or existing structure; rather, it is used by code-writing groups for recommend-

ing appropriate load and resistance safety factors for new structural design or evaluation specifications. One commonly used calibration approach is based on the principle that each type of structure should have uniform or consistent reliability levels over the full range of applications. For example, load and resistance factors should be chosen to produce similar  $\beta$  values for bridges of different span lengths, of differing numbers of lanes, of simple or continuous spans, of roadway categories, and so forth. Thus, a single target  $\beta$  must be achieved for all applications. On the other hand, some engineers and researchers are suggesting that higher values of  $\beta$  should be used for more important structures such as bridges with longer spans, bridges that carry more traffic, or bridges that, according to AASHTO, are classified as critical for “social/survival or security/defense requirements.” Because higher  $\beta$  levels would require higher construction costs, the justification should be based on a cost-benefit analysis whereby target  $\beta$  values are chosen to provide a balance between cost and risk (Aktas, Moses, and Ghosn, 2001). This latter approach is still under development in order to establish the proper criteria and methods for estimating appropriate cost functions.

In many code calibration efforts, appropriate target  $\beta$  values are deduced based on the performance of existing designs. That is, if the safety performance of bridges designed according to current standards has generally been found satisfactory, then the reliability index obtained from current designs is used as the target that any new design should satisfy. The aim of the calibration procedure is to minimize designs that deviate from the target reliability index. Such calibration with past performance also helps to minimize any inadequacies in the database, a minimization that has been previously reported by Moses and Ghosn (1985). It was found that the load and resistance factors obtained following a calibration based on “safe existing designs” are relatively insensitive to errors in the statistical data base as long as the same statistical data and criteria are used to find the target reliability index and to calculate the load and resistance factors for the new code. In fact, a change in the load and resistance statistical properties (e.g., in the coefficients of variation) would affect the computed  $\beta$  values for all the bridges in the selected sample population of existing bridges and, consequently, their average  $\beta$  value. Assuming that the performance history of these bridges is satisfactory, then the target reliability index would be changed to the new “average,” and the calibrated load and resistance factors that would be used for new designs would remain approximately the same.

The calibration effort is usually executed by code groups as follows:

- Reliability indexes are calculated for a range of bridge configurations that satisfy current code design criteria deemed to produce satisfactory performance. The calculation is based on statistical information about the

randomness of the strength of members, the statistics of load intensities, and their effects on the structures.

- In general, there will be considerable scatter in such computed reliability indexes. If the existing code is believed to provide an average satisfactory performance, a target  $\beta$  can then be directly extracted. This is done by examining the performance and experience of selected bridge examples and averaging the  $\beta$  values.
- For the development of new design codes, load and resistance factors and nominal design loads (or return periods) are selected by trial and error to satisfy the target  $\beta$  as closely as possible for the whole range of applications.

To execute the calculation of the reliability index, one needs to obtain the statistical data for all the random variables that affect the safety margin  $Z$  of Equation 2.3, including all the uncertainties in estimating the variables that describe the member resistances and the load effects. Experimental and simulation studies have developed statistical estimates of member resistances for different types of bridge structural members. These models have accounted for the variability and uncertainties in estimating the material properties, modeling errors, differences between predicted member capacities and measured capacities, human error, and construction control. For example, Nowak (1999) followed the approach of Ellingwood et al. (1980) and represented a bridge member resistance capacity by a variable  $R$  that is the product of several variables, such that

$$R = M F P R_n \quad (2.8)$$

where

- $M$  = material factor representing properties such as strength, modulus of elasticity, capacity to resist cracking, and chemical composition;
- $F$  = fabrication error including geometry, dimensions, and section modulus;
- $P$  = analysis factor such as approximate models for estimating member capacity, idealized stress and strain distribution models; and
- $R_n$  = predicted member capacity using code-specified methods.

Equation 2.8 can be used to find the mean of  $R$  using Equation 2.2 if the total resistance bias,  $b_r$ , is set to be equal to the product of the mean values of  $M$ ,  $F$ , and  $P$ .

In addition it is possible to add a system factor,  $\lambda_{\text{sys}}$ , that represents the capacity of the “system” to continue to carry loads after the failure of the first member. Thus, the system capacity,  $R_{\text{sys}}$ , may be represented as follows:

$$R_{\text{sys}} = \lambda_{\text{sys}} M F P R_n \quad (2.9)$$

The resistance model of Equations 2.8 and 2.9 does not directly account for member deterioration or other changes

with time. Thus, all the variables are time-independent random variables.

For a bridge member (or structural system) to be safe, the resistance should be large enough to withstand the maximum load effect that could occur within the structure’s service life. Estimating the effects of the maximum loads involves a number of random variables, which may often be associated with large levels of modeling uncertainties. In particular, the intensities of the maximum loads are time-dependent random variables in the sense that longer service lives imply higher chances that the structure will be subjected to a given extreme load level. On the other hand, the projection of limited load intensity data, collected from previous measurements over short periods of time, to future return periods is associated with various levels of statistical modeling uncertainties. In addition, modeling the structure’s response to the applied loads and estimating the variables that control the effects of the loads on the structure are associated with high levels of uncertainty that are independent of the return period. These modeling uncertainties are often represented by time-independent random variables. Thus, the effect of a particular load type,  $i$ , on a structural member may be represented by an equation of the form

$$S_i = \lambda_i f_i (\lambda_{Q_i} C_{ji} Q_i) \quad (2.10)$$

where

- $S_i$  = the load effect for load type  $i$ ;
- $\lambda_i$  = the analysis modeling factor that accounts for differences between measured load effects and predicted load effects;
- $f_i(\cdot)$  = the analysis prediction model that converts load intensities into load effects;
- $Q_i$  = the projected intensity variable of load type  $i$  for the return period of interest;
- $\lambda_{Q_i}$  = the statistical modeling variable that accounts for the limitations in predicting the value of  $Q_i$ ; and
- $C_{ji}$  = the analysis variables such as bridge material and geometrical properties required for executing the analysis for load type  $i$ .

Several such variables, each represented by the index,  $j$ , may be required to execute the load effect analysis. As mentioned above, all the variables in Equation 2.10 may be considered random where  $Q_i$  is a time-dependent random variable and the remaining variables are time-invariant.

The probability density of the load intensity,  $Q_i$ , for a given return period,  $t$ , can be calculated by studying the probability that  $Q_i$  will exceed a given value within  $t$ . Assuming that the occurrence of load events follows a Poisson model, the probability that the load intensity will exceed a value  $x$ , within a period,  $t$ , is represented by  $(1 - F_{Q_i,t}[x])$ , which may be approximated as

$$\Pr(Q_i > x; T < t) = 1 - F_{Q_i,t}(x) = 1 - e^{(-\lambda t)} \quad (2.11)$$

where  $p$  is the rate of exceedance per unit time.  $p$  is equal to the probability of exceeding  $x$  when  $t$  equals 1.0:

$$p = \Pr(Q_i > x) = 1 - F_{Q_i}(x). \quad (2.12)$$

For extreme values of  $x$  when the values of  $F_{Q_i}(x)$  are close to 1.0, and when  $p$  is calculated for one unit of time while the return period,  $t$ , consists of  $m$  units of time, Equation 2.11 can be approximated as

$$\Pr(Q_i > x; T < t) = 1 - F_{Q_i,t}(x) = 1 - e^{(-tp)} \approx 1 - (1 - p)^m \quad (2.13) \\ = 1 - (F_{Q_i}(x))^m$$

or

$$\Pr(Q_i < x; T < t) = F_{Q_i,t}(x) \approx F_{Q_i}(x)^m \quad (2.14)$$

In other words, Equation 2.14 indicates that the cumulative probability function for a return period of time,  $t$ , may be approximated by raising the cumulative probability function of the basic time period to the power,  $m$ . For example, assuming that  $F_{Q_i}(x)$  is the probability distribution of  $Q_i$  for 1 day, the probability distribution for a return period of 100 days can be calculated from Equation 2.11 or Equation 2.14 by setting  $m$  equal to 100. On the other hand, if  $F_{Q_i}(x)$  is the probability distribution for one event, then assuming  $n$  events per day, the probability distribution of the load intensity for a 100-day return period is calculated by setting  $m$  equal to  $100n$ .

Equations 2.11 through 2.14 are valid for studying the effect of one individual load of type  $i$ . However, the probability that two or more load events will occur simultaneously within the service life of the structure is a function of the rate of occurrence of each event, the time duration of the events, and the correlation between the events. Even when two load types can occur simultaneously, there is little chance that the intensities of both events will simultaneously be close to their maximum lifetime values. Therefore, the reliability calculations must account for all the random variables associated with estimating the maximum values of each load type and the possibility of load combinations. Available methods for studying the load combination problem have been discussed in Chapter 1. In particular, the Ferry-Borges model that is used in this study is described in detail in Section 2.5.

In order to execute the reliability calculations based on the Ferry-Borges model, statistical data on structural member and structural system resistances as well as data on the load intensities, their rate of occurrence, and their time duration are required. In addition, the uncertainty in modeling the effect of the loads on the structures should be considered. The next two sections give summaries of the statistical models used in this study based on the work available in the reliability literature. The models used are adopted from previous studies that led to the development of bridge design specifications or other structural design codes.

## 2.3 RESISTANCE MODELS

The object of this project is to study the reliability of highway bridges subjected to extreme load events and their combinations. In addition to live loads, the extreme events under consideration consist of wind loads, earthquake loads, ship collisions, and scour. Except for live loads and scour, all these events primarily produce horizontal loads on bridges. The bridge substructure consisting of the columns in a bridge bent and the foundation is the primary system that resists the applications of horizontal loads. The occurrence of scour, which is the erosion of the soil material around bridge piers, would also jeopardize the safety of the foundation system. Therefore, the focus of this study will be on the capacity of bridge substructures to resist the effect of lateral forces induced by the extreme events under consideration.

The intensities of the extreme load events are time-dependent random variables in the sense that the longer the bridge structure is operational, the higher the chances are that an extreme event with a high level of intensity will occur, causing the failure of the structure. In addition, as mentioned above, modeling the effect of these load events and the resistance capacity of the structure is associated with varying degrees of uncertainties because of the limitation of the analysis models that are commonly used as well as the difficulty of determining the exact properties of the structure and other factors that affect its behavior. The approach used in this study to account for these modeling uncertainties and material variability is by assuming that many of the factors that control the behavior and the response of bridges can be treated as random variables. The statistical uncertainties and the biases associated with estimating these variables are normally obtained from comparisons of analytical models with test results and by studying the data assembled from various measurements of material properties and bridge member and system responses. The object of this current project is not to collect such statistical data but to use the "most widely accepted" models for the needs of this study. A model is generally judged to be "acceptable" if it has been applied during recent code calibration efforts. This section provides a review of the structural and foundation resistance models that are used during recent studies dealing with the calibration of design codes or that are most commonly used in practice. These models will be adapted for use in this project to calibrate the load factors for the design of highway bridges and to study the reliability of such bridges when they are subjected to extreme events and combinations of extreme events.

### 2.3.1 Bridge Column Resistance Capacity

The concrete columns of a bridge bent are subjected to lateral loads from the extreme events as well as from vertical gravity loads caused by the permanent weight and live load.

The safety of a bridge column under combined axial loads and moment-causing lateral loads is defined by a  $P$ - $M$  interaction curve (axial load versus moment curve). Figure 2.2 shows a typical  $P$ - $M$  curve for a concrete column. In bridge engineering practice, most columns are designed such that the applied combined loading remains in the vicinity of the balanced point, that is, in the region in which the effect of the axial load does not significantly reduce the moment capacity of the column. For this reason, it is herein assumed that when the substructure is subjected to lateral loads, column failures will primarily be due to bending. Hence, the statistical data provided by Nowak (1999) for calibrating AASHTO LRFD resistance factors for bending of concrete members will be used when checking the safety of bridge columns subjected to lateral loads. When only vertical loads are applied, the dominant loading is axial compression. In this case, the model proposed by Ellingwood et al. (1980) will be used.

During the AASHTO LRFD calibration, Nowak (1999) used a bias of 1.14 and a COV of 13% for the moment capacity of reinforced concrete members. A “bias” is defined as the ratio of the mean value to the nominal or design value. This means that the average moment capacity of a bridge column will generally be different than the value calculated using the procedures outlined by the AASHTO LRFD code. There will also be a scatter in the moment capacities of columns designed to the same specifications and constructed following the same common construction procedures. The average value of these capacities will be 1.14 times the specified nominal capacity. “COV” is defined as the standard deviation divided by the mean value. Using Equation 2.1, a COV of 13% means that

the standard deviation will be equal to 0.148 ( $0.13 \times 1.14$ ) times the specified value. The biases and COVs, used during the AASHTO LRFD calibration, account for uncertainties in the material strength, geometric dimensions, and analysis. During the calibration process, Nowak (1999) used a lognormal probability distribution to model the member resistance and to describe the scatter of the bending moment capacities.

For axial loading of concrete columns, Ellingwood et al. (1980) used a lognormal distribution with a bias of 1.05 and a COV of 16%. When bridge columns are subjected to concentrated transverse forces such as when a ship or a barge collides into a column, the column may fail in shear. For shear failures of concrete columns Nowak (1999) uses a bias of 1.40 and a COV of 17% for columns with no steel shear reinforcement. When the columns are reinforced with steel, a bias of 1.2 and a COV of 15.5% are used.

The bending failure of one column in a multicolumn bent does not necessarily lead to the collapse of the substructure. In fact, Liu et al. (2001) have shown that multicolumn bents formed by columns confined with lateral reinforcing steel will, on the average, be able to withstand 30% additional load beyond the load that causes the first column to reach its ultimate bending capacity. The COV was found to be on the order of 12.5%. Substructure systems composed of unconfined multiple columns will on the average provide 15% more bending capacity with a COV of 8%. The distribution of the system’s modeling factor is assumed to be normal. This issue is further discussed in Section 2.3.3. The characteristics of the random variables describing the capacity of the columns of bridge substructures are summarized in Table 2.1.

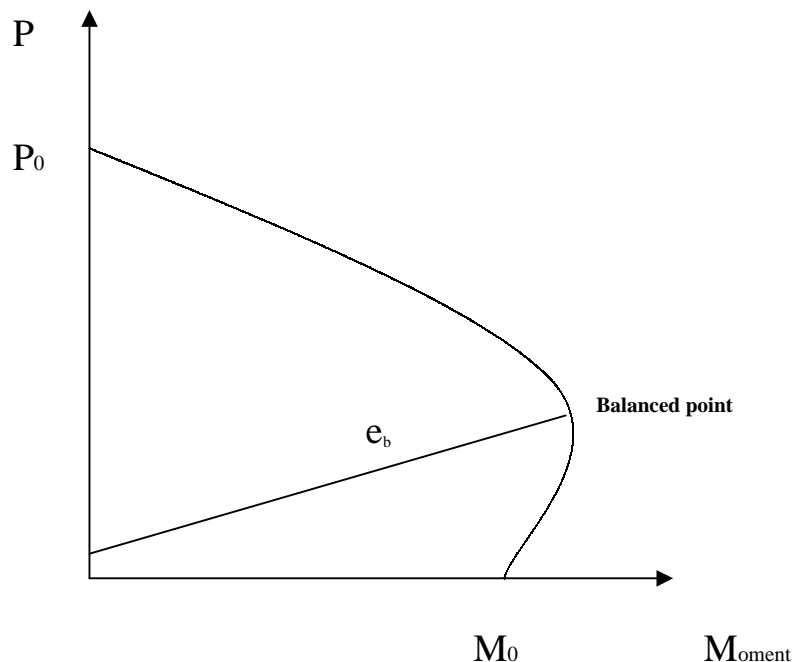


Figure 2.2. Strength interaction diagram for concrete columns.



**TABLE 2.1 Input data for concrete column capacity**

Variable	Bias	COV	Distribution Type	Reference
Moment capacity, $M_{col}$	1.14	13%	Lognormal	Nowak (1999)
Axial capacity, $P_{col}$	1.05	16%	Lognormal	Ellingwood et al. (1980)
Shear capacity no steel, $V_{col1}$	1.40	17%	Lognormal	Nowak (1999)
Shear capacity with steel, $V_{col2}$	1.20	15.5%	Lognormal	Nowak (1999)
System capacity for bending of unconfined multicolumn bents, $\lambda_{sys,u}$	1.15	8%	Normal	Liu et al. (2001)
System capacity for bending of confined multicolumn bents, $\lambda_{sys,c}$	1.30	12.5%	Normal	Liu et al. (2001)

### 2.3.2 Foundation/Soil Resistance Capacity

Another important failure mode that may jeopardize the safety of bridge substructures is the failure of the foundation system. This failure could be due to the failure of the foundation structural elements (e.g., piles) or failure in the soil. The capacity of the soil to resist failure is controlled by the specific weight of the soil; the type of soil material (e.g., clay or sand) and the depth; and the size and type of the foundation (e.g., footings on piles or pile shaft).

For most of the examples treated in this study, the foundation system is considered to be a drilled shaft pile in sands. This assumption is made in order to keep the analysis of the foundation reasonably simple and consistent with the overall objective of this study. The response of the column to lateral loads can then be modeled as shown in Figure 2.3. The simplified model used assumes an ultimate soil resistance capacity related to Rankine's passive pressure as described by Poulos and Davis (1980).

In Figure 2.3,  $F$  is the applied lateral force,  $e$  gives the height of the column above ground level,  $L$  is the foundation depth, and  $P_p$  is the passive resultant resisting force of the soil (produced by the triangular soil pressure resisting the motion). For long piles, the maximum bending moment in the pile shaft occurs at a distance  $f$  below the soil surface where the force from the soil pressure, up to depth  $f$ , is equal to the applied lateral force  $F$ . If  $f$  is larger than the foundation depth,  $L$ , the pile acts as a short pile, the controlling mode of failure is rigid overturning about the base of the pile, and the moment arm is  $H = L + e$ . This is shown in Figure 2.3(a). If  $f$  is smaller than  $L$ , then the maximum moment will occur at a depth  $f$ , and the controlling mode of failure is bending of the pile. In this case, the moment arm is  $H = f + e$  and the pile acts as if

it is fixed at a distance  $f$  below the soil level. This is shown in Figure 2.3(b).

According to Poulos and Davis (1980), the nominal active force  $P_p$  for sandy soils is given as

$$P_p = \frac{3\gamma DK_p L^2}{2} \quad (2.15)$$

where

$\gamma$  = the specific weight of sand,

$L$  = the depth of the pile,

$D$  = the diameter of the pile, and

$K_p$  = the Rankine coefficient, which is given by

$$K_p = \frac{1 + \sin(\phi_s)}{1 - \sin(\phi_s)} \quad (2.16)$$

where  $\phi_s$  is the angle of friction for sand.

When the depth of the soil is such that  $f < L$ , the pile system is simply an extension of the bridge column and can be treated in the same manner as the column, using the same bias and COV given by Nowak (1999) for bridge members in bending.

The dominant factors that control the safety of the soil are the specific weight of the soil, the angle of friction, and the modeling uncertainties associated with using the Rankine model. Poulos and Davis (1980) and Becker (1996) mention that for the lateral soil pressure on pile shafts, the Rankine model is conservative, providing a bias of about 1.5 when compared with measured data with a COV on the order of 20%. Becker (1996) also mentions that the specific weights

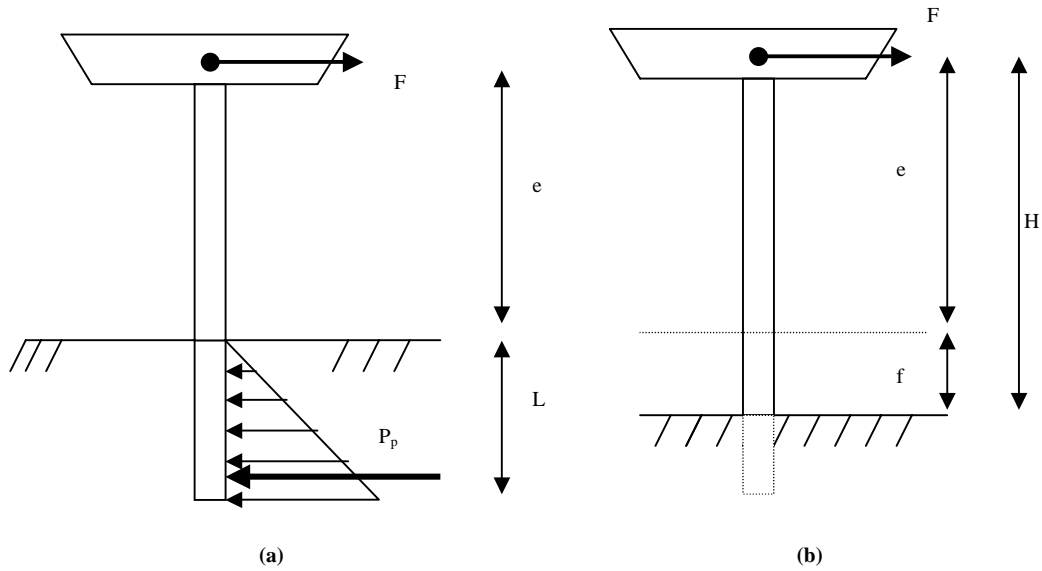


Figure 2.3. Free body diagram of bridge foundation system: (a) free body diagram for a short pile, dominant failure mode is tipping at base; (b) diagram for long pile, dominant failure mode is bending at distance  $f$  below soil level.

of soils will have variability with a COV equal to 7% compared with the measured value while estimates of angle of friction are associated with a COV of 13%. For the vertical bearing capacity, Poulos and Davis (1980) indicate that the applicable pile design formulas provide a bias of 1.0 when compared with pile tests with a COV on the order of 25%. Because most of the loads under consideration are dynamic in nature, it is proposed to follow the approach of Bea (1983) and apply a cyclic bias of 1.0 with a COV of 15% when analyzing the resistance of soils for foundations subjected to repeated cyclic forces. The primary random variables that control the estimation of the lateral soil resistance of the pile-

shaft system under lateral loads are summarized in Table 2.2. A normal distribution is assumed for all the random variables.

### 2.3.3 System Capacity

The analysis of multiple-column bents produces different moments in each column because of the effect of the dead load and the presence of axial forces. An extensive analysis of different bent configurations founded on different soil types was performed for NCHRP Project 12-47 (Liu et al., 2001). The results showed that, because of the load redistri-

TABLE 2.2 Input data for soil-related random variables

Variable	Bias	COV	Distribution Type	Reference
Unit weight of soil, $\gamma$	1.0	7%	Normal	Becker (1996)
Angle of friction, $\phi_s$	1.0	13%	Normal	Becker (1996)
Rankine earth pressure model for lateral force on piles, $K_p$	1.5	20%	Normal	Poulos and Davis (1980) Becker (1996)
Soil bearing capacity, $P_{soil}$	1.0	25%	Normal	Poulos and Davis (1980)
Cyclic effects, $\lambda_{cyc}$	1.0	15%	Normal	Bea (1983)

bution and the presence of ductility, multiple-column bents with confined concrete would on the average fail at loads up to 30% higher than the loads that make the first column reach its ultimate member capacity with a COV of about 12.5%. Systems with unconfined columns give system reserve ratios of about 1.15 (15% additional system capacity compared with first member capacity) with a COV of about 8%.

It is noted that system reserve ratio should be included to study the safety of the system (as compared with member safety) only for the cases in which a linear elastic analysis is performed. In the cases in which a full plastic analysis is performed, the system reserve is automatically taken into consideration.

## 2.4 LOAD MODELS

As mentioned earlier, the intensity of the extreme load events are time-dependent random variables in the sense that the longer the bridge structure is operational, the higher the chances are that an extreme event with a high level of intensity will occur causing the failure of the structure. However, modeling the effects of these loads is also associated with varying levels of uncertainties because of the limited available data, the limitations of the commonly used analysis models, and the difficulty of estimating the exact properties of the structure and other factors that affect its behavior. The approach followed in this project is to account for the analysis model uncertainties by assuming that many of the parameters that control the behavior and the response of bridges can be treated as random variables. The biases and COVs associated with estimating these variables are normally obtained from comparisons of analytical models to test results and by studying the data assembled from various measurements of bridge member and system responses. The object of this current project is not to collect such statistical data but to use “widely accepted” statistical models that have been applied during recent code calibration efforts for the needs of this study. This section provides a review of the models used in this study to calibrate the load factors for the design of highway bridges subjected to the combination of extreme events.

### 2.4.1 Gravity Loads

#### *Dead Loads*

The dead load biases and COVs used by Nowak (1999) during the reliability calibration of the AASHTO LRFD are

1. A bias of 1.03 with a COV of 8% for factory-made members,
2. A bias of 1.05 with a COV of 10% for cast-in-place members, and
3. For the wearing surface, a 88.9-mm (3.5-in.) average asphalt thickness along with a COV of 25%.

Nowak (1999) also assumes that the total load effect (live load + dead load) follows a normal distribution. Ellingwood et al. (1980) suggest that the dead load follows a normal distribution. In the calculations performed in this study, a common bias of 1.05 and a COV of 10% are used for the dead load using a normal distribution.

#### *Live Loads*

A major portion of the AASHTO LRFD calibration effort was spent on studying the effect of live loads. The statistical database for live loads was primarily obtained from truck weight histograms collected in Ontario (Nowak and Hong, 1991). Also, a limited set of weigh-in-motion data collected in Michigan (Nowak and Hong, 1991) and a weigh-in-motion study supported by FHWA (Goble et al., 1991) were available. Using the Ontario statistical database, Nowak (1999) calculated the target reliability index for member capacity,  $\beta_{\text{target}}$ , to be 3.5. This value is the average reliability index obtained for a representative sample of components of different bridge configurations designed to satisfy the AASHTO standard specifications (1996) with the HS-20 design load. Load and resistance factors were calibrated for the AASHTO LRFD using the same statistical database and using the 3.5 target value. The assumption of the code writers was that HS-20 bridges have performed satisfactorily under current live loading conditions and, thus, the new code should be calibrated to provide on the average a similar level of safety.

Only “heavy” trucks were measured in the Ontario survey. Nowak (1999) does not provide the actual truck weight histogram, but Moses (2001) found that the weights of the “heavy trucks” used in the AASHTO calibration effort approach a normal distribution with a mean of 300 kN (68 kips) and a standard deviation of 80 kN (18 kips) (COV = 26.5%). Nowak (1999) indicates that a typical site will have an average daily “heavy” truck traffic of about 1,000 trucks per day. Nowak (1999) also assumes that about 1 in every 15 “heavy” trucks will be side-by-side with another “heavy” truck. This produces a rate of side-by-side “heavy” truck occurrences on the order of 6.67%. On the other hand, data collected by Moses and Ghosn (1985) have shown that the truck population (for all trucks) on Interstate highways is on the order of 2,000 to 3,000 trucks per day (it may even reach 5,000 trucks per day in some cases) but that the percentage of side-by-side events for all the truck population is on the order of 1% to 3%. This percentage, however, may depend on site conditions and truck traffic volume. This comparison would indicate that Nowak’s data are highly biased toward the conservative side.

The statistics on truck weights (mean = 300 kN and standard deviation = 80 kN) and truck daily rates (1,000 trucks per day) are used to find the expected maximum truck load effect for different return periods using Equations 2.11 and 2.14. The calculations show that these statistics would produce results that replicate the results provided by Nowak

(1999) for the maximum extreme load effects for various return periods. Nowak (1999) does not provide the COVs for the different return periods that he considered, but the calculations using Equations 2.11 and 2.14 show that the COV for the truck load intensity decreases as the return period increases. Calculations for a 75-year return period using the mean truck weight of 300 kN and a standard deviation of 80 kN show that the 75-year maximum truck weight intensity that a bridge will be subjected to will be 734 kN (165 kips) with a COV less than 3%.

The 3% COV calculated above reflects the fact that for very long projection periods and for large number of truck occurrences, the chances that the bridge will be subjected to a high truck load become more certain assuming a high level of confidence in the input data base. On the other hand, because of statistical and modeling uncertainties, the final COV for the maximum combined load effects should be higher than 3%. For example, assuming two lanes of traffic, Nowak (1999) used a final COV for the truck load effects on the order of 19% to 20%. The final COV values used by Nowak (1999) account for the uncertainties in estimating the maximum live load, the load distribution to individual members, and the dynamic amplification factor. It is herein believed that this 19% associated with a bias of 1.0 must also account for the site-to-site variability (see Moses and Ghosn, 1985).

Although the final COV of 19% to 20% used by Nowak (1999) accounts for the uncertainty in estimating the dynamic amplification effects of moving vehicles on a flexible bridge superstructure, Nowak also gives the statistical information on the dynamic amplification factor separately. According to Nowak (1999), the measured dynamic effect (dynamic amplification factor) has a mean value equal to 9% of the static effect for two lanes of traffic with a COV of 6%. For one lane of traffic, the dynamic amplification factor is 13% of the static loads with a COV of 10%.

Given a 75-year maximum expected truck intensity COV of 3%, a dynamic amplification COV of 10%, and a final COV of 19% to 20%, it is concluded that the modeling uncertainties including site-to-site variability are associated with a COV on the order of 18%. A lognormal distribution is used to represent the modeling uncertainties because these involve the multiplicative effects of several factors including an axle distribution factor that accounts for different truck configurations, an analysis uncertainty factor, a statistical uncertainty factor, and a site-to-site variability factor (see also Moses and Ghosn, 1985).

The HL-93 live load model of the AASHTO LRFD specifications (1998) is intended for a 75-year design life. Several tables provided by Nowak (1999) give the bias between the projected maximum 75-year effects for one lane of traffic and the HL-93 truck load effects for simple span and multi-span bridges. Because this project places emphasis on the reliability analysis of bridge bents, the focus is on multi-span bridges. Table B-16 of Nowak's report lists the variation of the bias as a function of the return period for the negative moment of two equal continuous spans. For the purposes of

this study, it is assumed that these biases are valid for all responses. In particular, the same biases of Table B-16 would be used for the reaction at the support. Trains of trucks rather than single occurrences control the loading of continuous span bridges. To extract the effect of one loading event, consisting of a train of trucks in one lane of traffic, the same approach proposed by Moses (2001) is followed. The purpose of the calculations is to find the bias for a single load event that would reproduce the results of Table B-16 of Nowak (1999) for one lane of traffic. Using Equations 2.11 and 2.14, it is found that the biases provided in Table B-16 of Nowak (1999) for the different return periods are exactly matched if the one load event is assumed to follow a normal distribution and is associated with a bias of 0.79 with a COV of 10%. The calculations assume that there will be 1,000 loading events each day with each loading event consisting of a train of trucks in one lane of traffic. The 0.79 bias is relative to the effect of one lane loading of the HL-93 live load model. For two lanes of traffic loaded simultaneously, the bias relative to the effect of one lane loading of the HL-93 model is found to be 1.58 with a COV of 7%. The calculations assume that there will be 67 events of two lanes loaded simultaneously. Using Equation 2.11 and 2.14, it is found that the two-lane loading will produce a 75-year maximum load effect equal to  $2 \times 0.88 (= 1.76)$  times the load effect of one lane of traffic. The  $2 \times 0.88$  factor is similar to the factor reported by Nowak (1999), who has suggested that a factor equal to  $2 \times 0.85 (= 1.70)$  gives a reasonable approximation to the effect of two-lane traffic relative to one-lane traffic.

In summary, to perform the reliability calculations for the needs of this study, the following assumptions are made:

1. A "heavy" truck loading event will, on the average, consist of a truck with a weight of 300 kN (68 kips) and a standard deviation of 180 kN (8 kips) (COV = 26.5%). In a typical day, there will be 1,000 "heavy loading events" (i.e., the rate of occurrence is 1,000 events per day).
2. Two side-by-side "heavy" truck events will occur at a rate of 67 events per day (i.e., 1,000/15) and, on the average, the weights of the two trucks will be 600 kN (136 kips) with a COV of 19%.
3. Multispan bridges will be subjected to 1,000 one-lane load events per day with a mean load effect value equal to 0.79 times the effect obtained from the HL-93 loading. The COV for one-lane load effects is 10%.
4. Multilane multi-span bridges will be subjected to 67 two-lane load events with a mean value equal to 1.58 times the effect obtained from one HL-93-lane load. The COV for two-lane load effects is 7%.
5. The dynamic amplification factor for one lane of traffic is 1.13 with a COV of 10%. For two lanes of traffic, the amplification factor is 1.09 with a COV of 6%.
6. A modeling variable is used with a mean value of 1.0 and a COV of 18%.
7. The truck load effects and dynamic factors are assumed to follow normal distributions as suggested by Nowak

(1999). The modeling variable is assumed to follow a lognormal distribution.

The live load model proposed in this section provides results that are consistent with the database used by Nowak (1999) when calibrating the AASHTO LRFD specifications. These are summarized in Table 2.3. It is noted that the dead load, the live load modeling factor, and the dynamic amplification factors are all time-independent random variables. Only the intensity of the applied live load will increase with the bridge's exposure period.

## 2.4.2 Earthquakes

The analysis of the response of a bridge structure to earthquakes involves a number of random variables. These variables are related to the expected earthquake intensity for the bridge site; the number of earthquakes at the site; the natural period of the bridge system; the spectral accelerations for the site, including soil properties; the nonlinear behavior of the bridge system; and the modeling uncertainties associated with current methods of analysis. The emphasis of the analyses performed in this project is on the horizontal motion of bridge bents caused by earthquakes. A discussion on each variable follows.

### *Intensity of Earthquake Accelerations*

The USGS mapping project developed maps providing the peak ground accelerations (PGAs) at bedrock level for various sites throughout the United States in terms of the proba-

bility of exceedance in 50 years (Frankel et al., 1997). These maps are available for probabilities of exceedance of 2% and 10% in 50 years. The 2% probability of exceedance in 50 years corresponds to an earthquake return period of about 2,500 years. The 10% in 50 years corresponds to a return period of about 500 years. These return periods are normally used as the bases of current bridge design practice. The probabilities of exceedance in 50 years can directly be related to the maximum yearly earthquake levels using Equations 2.11 or 2.14. In addition, Frankel et al. (1997) provide a number of curves describing how the probability of exceedance in 1 year varies as a function of PGA for a number of sites. Figure 2.4 gives the yearly probability of exceedance for a range of PGAs and for a number of representative sites provided by Frankel et al. (1997) for the areas with the following zip codes: 10031 in New York City, 38101 in Memphis, 55418 in St. Paul, 98195 in Seattle, and 94117 in San Francisco.

### *Rate of Earthquake Occurrences*

The number of earthquakes varies widely from site to site. The USGS mapping project also provides the expected number of earthquakes at particular sites. For example, the average number of earthquakes in 1 year for the five earthquake sites listed above varies from about 8 per year to 0.009 per year. For example, San Francisco may be subjected to about 8 earthquakes per year while Seattle may be subjected to 2 earthquakes. The rates for the other sites are usually less than 1.0: Memphis will witness one every 2 years (yearly rate = 0.50), New York City one every 2.5 years (yearly rate = 0.40), and St. Paul one in 111 years (yearly rate =  $9 \times 10^{-3}$ ).

**TABLE 2.3** Input data for dead and live load random variables

Variable	Bias	COV	Distribution Type	Reference
Dead load, $F_{DC}$	1.05	10%	Normal	Nowak (1999)
Live load modeling factor, $\lambda_{LL}$	1.0	18%	Lognormal	Moses and Ghosn (1985)
Live load multispan one event in one lane (relative to one lane of HL-93 load), $I_{LL,1}$	0.79	10%	Normal	Calculated based on Nowak (1999) and Moses (2001)
Live load one event in multilane (relative to one lane of HL-93 load), $I_{LL,2}$	1.58	7%	Normal	Calculated based on Nowak (1999) and Moses (2001)
Dynamic amplification one lane, $I_{IM,1}$	1.13 (=mean value)	10%	Normal	Nowak (1999)
Dynamic amplification two lanes, $I_{IM,2}$	1.09 (=mean value)	6%	Normal	Nowak (1999)

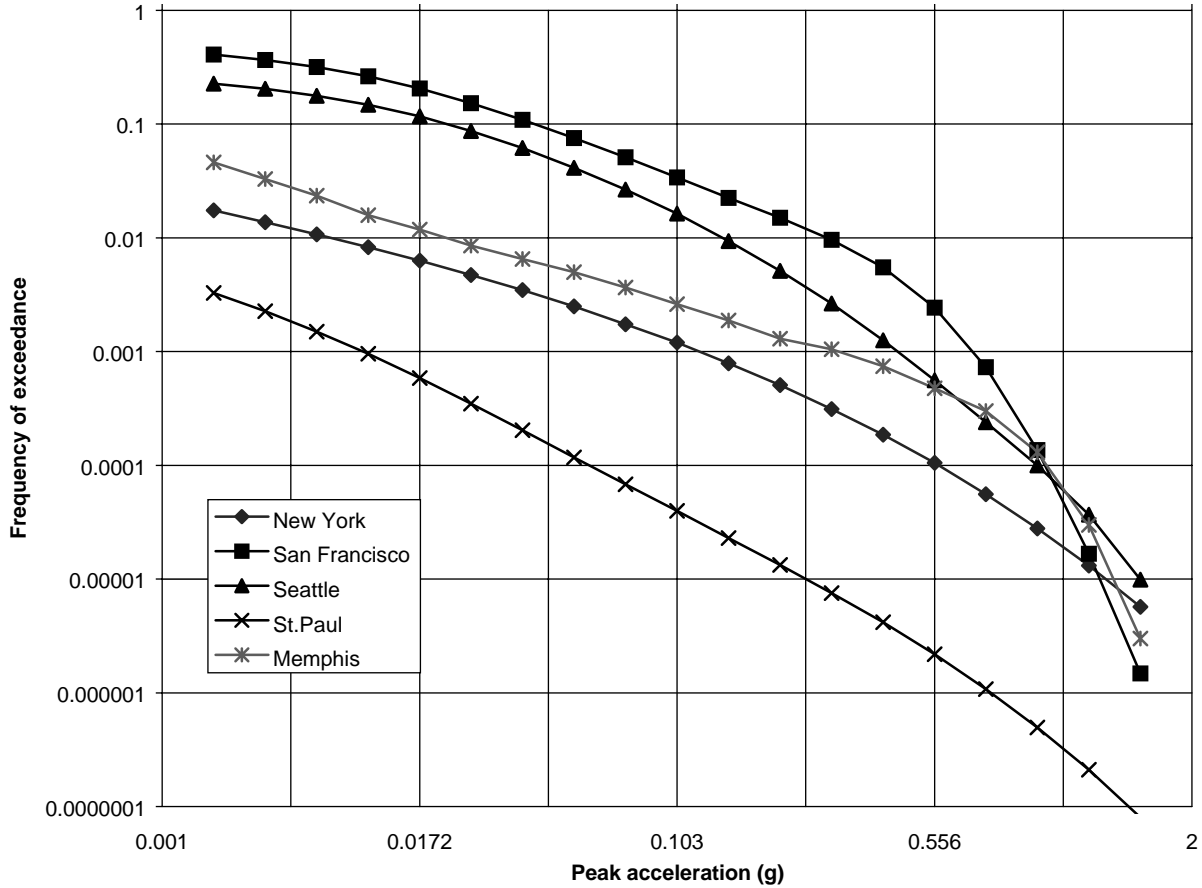


Figure 2.4. Annual probability of exceedance curves for PGA (based on USGS website).

### Natural Period of Bridges

The natural period of a bridge depends on many parameters, including the type and the characteristics of the bridge structure and bridge foundation and the stiffness of the soil. Takada, Ghosn, and Shinozuka (1989) have suggested that the average value of the period is about 1.08 times the value calculated using design methods (bias = 1.08) with a COV on the order of 20%. These values account for the soil-structure interaction (SSI) and other analysis effects. The values provided by Takada, Ghosn, and Shinozuka (1989) are primarily for buildings. The Takada, Ghosn, and Shinozuka (1989) data should be applied on structural models that did not include the effects of SSIs because the 1.08 bias accounts for the effects of SSI. Because the analysis model used in this study includes the effects of SSI, a lower bias should be used (Stewart, Seed, and Fenves, 1999).

When SSI models are included in the analysis (as is the case in the models used in this project), the variation between the measured periods and the predicted periods appears to be smaller, and the bias is reduced to a value close to 1.0 (Stewart, Seed, and Fenves, 1999). This phenomenon is shown in Figure 2.5, which is adapted from the paper by Stewart, Seed, and Fenves (1999). The ordinate of the fig-

ure gives the ratio of the difference between the predicted period,  $\hat{T}_{pre}$ , and the measured period,  $\hat{T}$ , divided by  $\hat{T}$ , where the periods account for the flexibility of the foundation because of SSI. The abscissa is the ratio of the structure height,  $h$ , over the product of the soil shear-wave velocity,  $V_s$ , times the measured period of the fixed structure,  $T$ . The abscissa is thus the inverse of the ratio of the soil-to-structure stiffness defined as  $\sigma$ . The figure shows that, on the average, the predicted periods accounting for SSI are reasonably similar to the values measured in the field. The bias is found to be 0.99 and the COV on the order of 8.5%. It is noted that the comparison is made for buildings rather than for bridges and that most of these sites had stiff soils. Also, the natural period of the fixed structural system,  $T$ , used in the abscissa is inferred from field measurements.

Chopra and Goel (2000) developed formulas for estimating the natural periods of buildings based on measured data. The spread in the data shows a COV on the order of 20% for concrete buildings and slightly higher (on the order of 23%) for steel frame buildings. Haviland (1976) suggested that a bias of 0.90 and a COV of 30% are appropriate for the natural period of structural systems.

Based on the review of the above references, it is herein decided to use a bias of 0.90 and a COV of 20% for the period

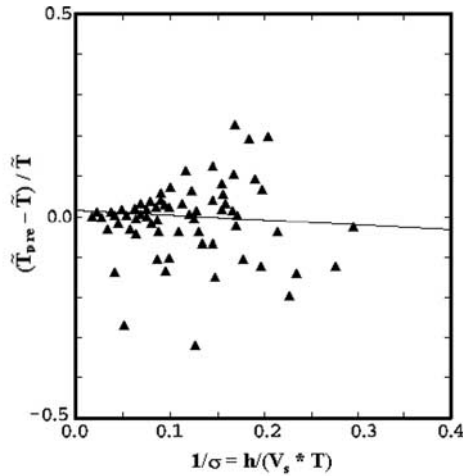


Figure 2.5. Variation of predicted natural period of structural systems including SSI compared with measured values (based on Stewart, Seed, Fenves, 1999).

of the system. The 0.90 bias, similar to that observed by Haviland (1976), is justified based on the fact that the analysis performed to calculate the period of the bridge system uses the nominal value for the modulus of elasticity of the concrete,  $E_c$ . In reality, the actual modulus of the concrete will be higher than the nominal value and, thus, the predicted stiffness larger than the actual stiffness, producing a lower actual period than predicted. A correction factor of 1.20 to 1.30 on the concrete modulus is often used in engineering practice that would justify the 0.90 bias ( $0.90 \approx 1/\sqrt{1.25}$ ). The COV of 20% used herein corresponds to the values observed by Chopra and Goel (2000) for buildings and the value used by Takada, Ghosn, and Shinozuka (1989). Also, the 20% COV provides an average value between the COV values from the various references studied. It may be argued that the prediction of the period for bridges may be less uncertain than that for buildings. However, the data collected by the various researchers cited in this section did not indicate any appreciable difference in the level of uncertainty because of building heights or sizes. Thus, it may be reasonable to assume that the COV on the period for bridges is also on the order of 20%. The proposed bias and COV are meant to account for both the uncertainties in the structural properties and the SSI parameters.

#### Mass Applied on the Column

The dead weight effect on bridge members was found by Nowak (1999) to be on the order of 1.05 times the nominal (design) weight with a COV of 10%. This COV, however, reflects the effects of the structural analysis and the uncertainty in estimating the weight. To account for the uncertainty in the weight alone, a COV of 5% is used. The probability distribution is assumed to be normal following the models used by Ellingwood et al. (1980) and Nowak (1999). The

variability in the mass and the weight considered here are used for calculating the earthquake inertial forces.

#### Seismic Response Coefficient

The USGS mapping project (Frankel et al. 1997) provides spectral accelerations for different sites within the United States. The spectral accelerations are given for periods of 0.2, 0.3, and 1.0 sec. Table 2.4 lists these values along with the corresponding PGAs for different sites. The sites considered are for the following zip codes: 10031 in New York City, 38101 in Memphis, 55418 in St. Paul, 98195 in Seattle, and 94117 in San Francisco. The spectral accelerations provided in Table 2.4 are for single-degree-of-freedom (SDOF) systems founded on bedrock. The values are given for only three natural periods—namely, 0.2, 0.3, and 1.0 sec—in addition to the PGA. The values shown in Table 2.4 are in %  $g$  where  $g$  is the acceleration caused by gravity. The spectral accelerations are given for a probability of exceedance of 2%, 5%, and 10% in 50 years.

NEHRP (1997) proposed a method to use the information provided in Table 2.4 to develop acceleration response spectra that are valid for systems with different natural periods. The NEHRP response spectra can be described by curves with the shape shown in Figure 2.6. In Figure 2.6, the ordinate gives the final normalized spectral acceleration,  $S_a$  (normalized with respect to  $g$ ), and the abscissa is the natural period of the system,  $T$ .  $S_{D_s}$  is the maximum spectral acceleration that is the spectral acceleration for the short period  $T_s = 0.2$  sec.  $S_{D_1}$  is the spectral acceleration for a period  $T_1 = 1$  sec. All spectral accelerations are given in function of the acceleration due to gravity,  $g$ .  $T_0$  gives the period at which the maximum spectral acceleration is reached.  $T_s$  gives the period at which the spectral acceleration begins to decrease below the maximum value. When the period  $T$  is less than  $T_0$ , the spectral acceleration increases linearly. When the period  $T$  is greater than  $T_s$ , the spectral acceleration is inversely proportional to  $T$ . The values of  $S_{D_s}$  and  $S_{D_1}$  are obtained from the spectral accelerations given in Table 2.4 adjusted to account for the site's soil properties.

The site soil coefficients are obtained from the NEHRP provisions as  $F_a$  for short periods and  $F_v$  for 1 sec from Table 4.1.2.4.a and 4.1.2.4.b of NEHRP (1997). NCHRP Project 12-49 (ATC and MCEER, 2002) is proposing to use a modification on the NEHRP spectra such that the maximum earthquake spectral response accelerations for short-period (0.2-sec)  $S_{D_s}$  and for the 1-sec period  $S_{D_1}$ , adjusted for the proper soil profile, are obtained from

$$S_{D_s} = F_a S_s \quad \text{and} \quad S_{D_1} = F_v S_1. \quad (2.17)$$

Critical periods on the response spectrum (see Figure 2.6) are obtained from

$$T_0 = 0.20 S_{D_1} / S_{D_s} \quad \text{and} \quad T_s = S_{D_1} / S_{D_s}. \quad (2.18)$$

**TABLE 2.4 Probabilistic ground motion values, in %g, for five sites (USGS website)**

	10% PE in 50 Yr	5% PE in 50 Yr	2% PE in 50 Yr
<b>San Francisco</b>			
PGA	52.65	65.00	76.52
0.2 sec $S_a$	121.61	140.14	181.00
0.3 sec $S_a$	120.94	140.44	181.97
1.0 sec $S_a$	57.70	71.83	100.14
<b>Seattle</b>			
PGA	33.77	48.61	76.49
0.2 sec $S_a$	75.20	113.63	161.34
0.3 sec $S_a$	62.25	103.36	145.47
1.0 sec $S_a$	22.06	32.23	55.97
<b>St. Paul</b>			
PGA	0.76	1.31	2.50
0.2 sec $S_a$	1.82	3.17	5.63
0.3 sec $S_a$	1.61	2.72	4.98
1.0 sec $S_a$	0.73	1.38	2.66
<b>New York</b>			
PGA	6.32	11.92	24.45
0.2 sec $S_a$	12.59	22.98	42.55
0.3 sec $S_a$	9.42	16.64	31.17
1.0 sec $S_a$	2.85	5.11	9.40
<b>Memphis</b>			
PGA	13.92	30.17	69.03
0.2 sec $S_a$	27.46	58.71	130.03
0.3 sec $S_a$	20.38	43.36	110.62
1.0 sec $S_a$	6.46	15.47	40.74

The equation describing the acceleration response spectrum,  $S_a$ , shown in Figure 2.6 can be expressed as

$$S_a = 0.6 \frac{S_{DS}}{T_0} T + 0.40 S_{DS} \quad \text{for } T < T_0,$$

$$S_a = S_{DS} \quad \text{for } T_0 < T < T_s,$$

(2.19)

and

$$S_a = \frac{S_{D1}}{T} \quad \text{for } T > T_s$$

The design spectra proposed by NCHRP Project 12-49 as adopted from NEHRP are based on the average response spectra developed by Frankel et al. (1997) from a large earthquake mapping project. Frankel et al. (1997) found that the level of confidence in the NEHRP spectra is related to the number of earthquakes recently observed as well as the knowledge of the type and locations of the faults in a particular region. For sites at which a large number of earthquakes were observed, the

COV is low; the COV is high for sites with few observed tremors. Frankel et al. (1997) provided maps showing uncertainty estimates for selected cities derived from Monte Carlo simulations. The data provided in this map show that the ratio between the 85th fractile and the 15th fractile for New York

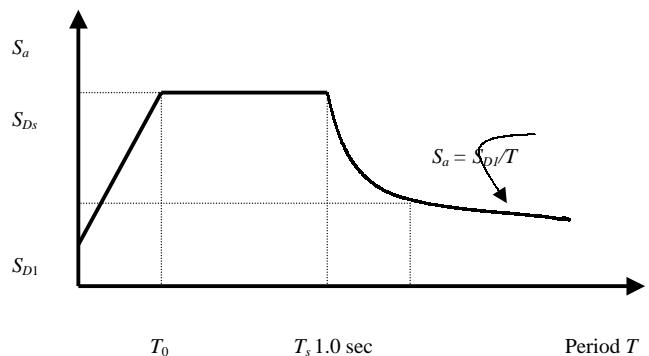


Figure 2.6. NEHRP response spectrum.



City is on the order of 5. Assuming a normal distribution, this means that the COV would be on the order of 30%. For the Memphis area, the ratio of the two fractiles is about 3, resulting in a COV of about 25%. For San Francisco, the projected COV is about 15%, and for St. Paul and Seattle the projections are that the COVs would be about 40% and 25%, respectively. Frankel et al. (1997) also show that the mean value of the spectral accelerations is very close to the uniform hazard spectra they developed and that resulted in the NEHRP specifications. It is noted that these observations are within the range of the values reported by Seed, Ugas, and Lysmer (1976), who observed that the results of dynamic analyses using a variety of earthquake records resulted in a range of spectral responses with a COV of about 30% from the average spectra.

In summary, this study will assume that the mean spectral accelerations are equal to the design spectral accelerations proposed in NCHRP Project 12-49 (i.e., bias = 1.0) with a COV that depends on the frequency of earthquakes at the site. Thus, the COV varies between 15% for San Francisco and 40% for St. Paul. The spectral accelerations are also assumed to follow normal distributions.

### *Response Modification Factor*

The response modification factor is related to the ductility of the system. The purpose of the response modification factor is to allow for a linear elastic analysis of structural systems although the system may exhibit large levels of plastic deformations. In fact, because earthquakes produce displacements rather than actual forces, traditional design of bridges for earthquakes allows bridge columns to reach their ultimate member capacity as long as the ductility capacity is not exceeded. To simplify the design and safety evaluation process, the ductility capacity,  $\mu_{\text{cap}}$ , of a concrete column is modeled through a response modification factor,  $R$ . The response modification factor is used to allow the designer to perform a linear elastic analysis and to check the safety of the column members for a modified moment capacity equal to  $R_m$  times the actual moment capacity of the column. Hence, if the applied moment assuming linear elastic behavior is lower than  $R_m$  times the actual moment capacity, the column is considered to be safe.

Analytical research studies have concluded that the response modification factor  $R_m$  is directly related to the ductility capacity  $\mu_{\text{cap}}$ . Thus, the response modification for a member, assuming an SDOF system, may be estimated if the member's ductility capacity,  $\mu_{\text{cap}}$ , is known. Miranda (1997) found that for typical periods of bridge systems (0.5 to 1.5 sec) subjected to a representative sample of earthquake records, the response modification,  $R_m$ , is on the average equal to the bridge column ductility capacity ( $R_m = \mu_{\text{cap}}$ ) with a COV of about 25%. This observation confirms the model first proposed by Newmark and Hall (1973) that was based on limited data from the El Centro Earthquake. The results of Miranda (1997) were calculated

for a variety of sites with a range of soil classifications. Liu et al. (1998) in a report to the National Center Earthquake Engineering Research (NCEER) and FHWA found that the COV reduces to about 17% if the earthquake records were chosen to match those that produce the design spectral accelerations.

In addition to the issue of the relation between  $R_m$  and  $\mu_{\text{cap}}$ , another issue concerns the level of uncertainty associated with estimating the ductility capacity  $\mu_{\text{cap}}$ . Results given by Priestley and Park (1987) show that the real ductility of bridge columns is on the average about 1.5 times higher than the ductility estimated from the design formulas with a COV of about 30%. Thus, using the results of Priestley and Park (1987) and Liu et al. (1998), the actual response modification factor,  $R_m$ , will be on the average 1.5 times the specified ductility capacity,  $\mu_{\text{specified}}$ , (bias of  $R_m = 1.5$ ) with a COV of 34% ( $0.90 \approx 1/\sqrt{1.25}$ ). The probability distribution for  $R_m$  is assumed to be normal.

The last issue with the response modification factor concerns the range of values specified for use during the design process by AASHTO and other earthquake design codes. For example, it is noted that the response modification factor,  $R$ , specified by AASHTO for use during the analysis of single-column bents is set at 2.0, while  $R_m = 3.5$  is used for multiple-column bents of essential structures. Also, values of 3.0 and 5.0 are used for "other structures." On the other hand, NCHRP Project 12-49 is proposing a single value,  $R_m = 6.0$ , for life safety for single-column and multicolumn bents and  $R_m = 1.5$  to secure proper operation. ATC-6 mentions that an  $R_m = 2.0$  is recommended for a wall-type pier "based on the assumption that a wall pier has low ductility capacity and no redundancy."

It is clear that the difference between the 2.0, 3.0, 3.5, 5.0, and 6.0 values of  $R_m$  used for the design of columns is not intended to account for the differences in the ductility capacities of the columns. Rather, the use of different values of  $R_m$  is meant to provide certain types of structures (particularly nonredundant and essential bridges) with higher levels of safety. In fact, since in all cases the design and construction procedures of columns in single-column bents or multicolumn bents are fairly similar, one would expect to find the ductility capacities of all columns to be about the same. It is noted that previous recommendations for the design of bridges under earthquake loads recommended that a response modification factor  $R_m = 8$  be used. In addition, tests on bridge columns performed at the University of Canterbury (Zahn, Park, and Priestley, 1986) have shown that the ductility of properly confined columns can easily exceed 7.5, although some damage would be expected to occur.

Based on the information collected from the references mentioned above, this study will assume that the ductility level of confined concrete columns can be modeled by a response modification factor  $R$  that has an average value  $\bar{R}_m$  of 7.5 and a COV of 34%. The probability distribution for  $R_m$  is assumed to be normal. It is noted that the values used herein are somewhat similar to those used by Hwang, Ushiba, and Shinozuka

(1988), who have recommended the use of a median value for  $R_m$  of 7.0 for shear walls with a COV of 40%. The use of a response modification factor during the analysis and design of bridge substructures implies that the design and safety evaluation account for the nonlinear capacity of the system. Thus, the reliability indexes calculated are for the system capacity rather than for member capacity.

*Modeling Factor*

The dynamic structural analysis produces a level of uncertainty in the final estimate of the equivalent applied forces and moments on a bridge substructure. These factors are due to the effects of lateral restraints from the slab, the uncertainty in predicting the tributary area for the calculation of mass, the point of application of the equivalent static load, the variability in soil properties and the uncertainty in soil classification, the effect of using a lumped mass model, the level of confidence associated with predicting the earthquake intensity, and so forth. Ellingwood et al. (1980) assumed that the modeling factor has a mean value equal to 1.0 and a COV on the order of 20% for buildings. The same value is used in these calculations.

Using the information provided in this section, the equivalent force applied on a bridge structure may be calculated using the following expression:

$$F_{apl} = \lambda_{eq} C' S_a(t'T) * \frac{A * W}{R_m} \tag{2.20}$$

where

- $F_{apl}$  = the equivalent applied force;
- $\lambda_{eq}$  = the modeling factor for the analysis of earthquake loads on bridges;

- $C'$  = the response spectrum modeling parameter;
- $A$  = the maximum 75-year peak ground acceleration at the site (a 75-year design life is used in order to be consistent with the AASHTO LRFD specifications);
- $S_a$  = the calculated spectral acceleration, which is a function of the period  $T$ , where  $T$  is the bridge column period and the period modeling factor,  $t'$ ;
- $W$  = the weight of the system;
- $R_m$  = the response modification factor; and
- $C'$  and  $t'$  = modeling parameters that express the variation of the true spectrum from the design spectrum and the true natural period of the system from the design period.

The statistical data used in the reliability analysis for the random variables of Equation 2.20 are summarized in Table 2.5. The parameters not listed in Table 2.5 are assumed to be deterministic. It is noted that all the random variables except for the earthquake intensity are time independent in the sense that they are not affected by the exposure period. The earthquake intensity is time dependent because the longer a bridge’s design life is, the higher the expected earthquake intensity that it will be exposed to. Finally, it is also noted that earthquakes last for short periods of time—a few seconds. In this study, for the sake of obtaining conservative results, it will be assumed that earthquakes will last about 30 sec ( $1/2$  min), during which time the response of the bridge will continuously be at its maximum value. Table 2.5 shows the mean and COV for the maximum yearly earthquake acceleration intensities of the five sites depicted in Figure 2.4. A comparison between the COV of the earthquake intensities and the COVs of the other variables demonstrates the dominance of the uncertainties in estimating the maximum acceleration during the reliability analysis.

**TABLE 2.5 Summary of input values for seismic reliability analysis**

Variable	Bias	COV	Distribution Type	Reference
Earthquake modeling, $\lambda_{eq}$	1.0	20%	Normal	Ellingwood et al. (1980)
Spectral modeling, $C'$	1.0	Varies per site (15% to 40%)	Normal	Frankel et al. (1997)
Acceleration, $A$	<i>San Francisco</i>	1.83% g (yearly mean)	from Figure 2.4	USGS website
	<i>Seattle</i>	0.89% g (yearly mean)		
	<i>Memphis</i>	0.17% g (yearly mean)		
	<i>New York</i>	0.066% g (yearly mean)		
	<i>St. Paul</i>	0.005% g (yearly mean)		
Period, $t'$	0.90	20%	Normal	Chopra and Goel (2000)
Weight, $W$	1.05	5%	Normal	Ellingwood et al. (1980)
Response modification, $R_m$	7.5 (mean value)	34%	Normal	Priestley and Park (1987) and Liu et al. (1998)

### 2.4.3 Wind Load

As explained by Ellingwood et al. (1980), the wind load on bridge structures is a function of the expected wind speeds at the bridge site, pressure coefficients, parameters related to exposure and wind speed profile, and a gust factor that incorporates the effects of short gusts and the dynamic response of the structure. In general, the wind load ( $W$ ) may be represented by an equation of the form

$$W = cC_p E_z G (\lambda_V V)^2 \quad (2.21)$$

where

- $c$  = an analysis constant,
- $C_p$  = the pressure coefficient,
- $E_z$  = the exposure coefficient,
- $G$  = the gust factor,
- $V$  = the wind speed at the desired return period, and
- $\lambda_V$  = the statistical modeling factor that accounts for the uncertainty in estimating  $V$ .

The exposure coefficient depends on the type of terrain (e.g., urban area, open country), and  $G$  depends on the turbulence of the wind and the dynamic interaction between the bridge structure and the wind. In addition to the time-dependent randomness of the wind speed, uncertainties in the estimation of the other terms contribute to the overall variability in the wind load. Ellingwood et al. (1980) assumed that  $c$ ,  $C_p$ ,  $E_z$ , and  $G$  are all random variables that follow normal distributions. Their mean values are equal to the nominal design values as calculated from design specifications, that is, the best estimates of each variable should be used during the design process. The COVs for each of the random variables are as follows: for  $c$ , the COV is 5%; for  $C_p$ , the COV is 12%; for  $G$ , the COV is 11%; and for  $E_z$ , the COV is 16%. The random variables represented by  $c$ ,  $C_p$ ,  $G$ , and  $E_z$  are time-independent, meaning that they do not change with the design life (or the exposure period of the structure to wind loads). Table 2.6 summarizes the data for the random variables considered.

For the purposes of this study, the fluctuations of the wind load applied on the structure with time are modeled as shown in Figure 2.7. The average time duration of each wind was found by Belk and Bennett (1991) to vary from 2.2 h to 5.62 h, depending on the site, with an average duration of 3.76 h and a COV close to 11%. This study assumes that each wind will

last about 4 h, during which time the wind force remains constant at its maximum value. Belk and Bennett (1991) have also found that an average site will be subjected to about 200 winds per year, which is the value that is used in this project to study the load combination problem. For the sake of simplicity, the model used herein assumes independence between individual wind events. The statistical models for wind speed are discussed further below.

### Wind Speeds

Data on wind velocities, extreme wind events, and the effect of winds on structures are available in the engineering literature (e.g., see Whalen and Simiu, 1998). However, much of this work is still under development and has not been applied in structural design codes. For this reason, in this project we will focus on the work of Ellingwood et al. (1980), which led to the development of ANSI 58 and subsequently the ASCE 7-95 guidelines. The AASHTO LRFD specifications are also based on the models developed for ASCE 7-95. According to the AASHTO LRFD, the basic design wind speed of 160 km/h (100 mph) is associated with an annual probability of 0.02 of being exceeded (i.e., the nominal recurrence interval is about 50 years). This value is for an open terrain with scattered obstructions having heights generally less than 9.1 m (30 ft) (ASCE 7-95 Exposure C). According to the ASCE 7-95 basic wind speed map, the 160 km/h wind would be the expected maximum wind for a 50-year return period for East Coast regions such as Philadelphia and Washington, D.C. While interior regions would have a design wind speed of 145 km/h (90 mph), coastal regions such as Long Island and Rhode Island would require a design speed of 190 km/h (120 mph), whereas regions such as New York City and Boston would require 180 km/h (110 mph) design winds. The higher design wind speeds for the coastal regions are due to the occurrence of hurricanes. The design wind speed maps do not correspond to actual projected 50-year maximum wind speed but give conservative envelopes to the expected 50-year wind speeds. In fact, based on data collected by Simiu, Changery, and Filliben (1979) for annual maximum wind speeds and assuming that wind speeds follow a Gumbel Type I extreme value distributions, Ellingwood et al. (1980) developed the results shown in Table 2.7 for wind speeds at different sites in the interior region of the United States. Belk and Bennett (1991) performed a statistical analysis of the data col-

**TABLE 2.6 Summary of input values for wind reliability analysis**

Variable	Bias	COV	Distribution Type	Reference
Analysis factor, $c$	1.0	5%	Normal	Ellingwood et al. (1980)
Pressure coefficient, $C_p$	1.0	12%	Normal	Ellingwood et al. (1980)
Exposure coefficient, $E_z$	1.0	16%	Normal	Ellingwood et al. (1980)
Gust factor, $G$	1.0	11%	Normal	Ellingwood et al. (1980)
Wind velocity, $V$	from Table 2.7	from Table 2.7	Gumbel	Simiu et al. (1979)
Statistical variable, $\lambda_V$	1.0	7.5%	Normal	Simiu et al. (1979)

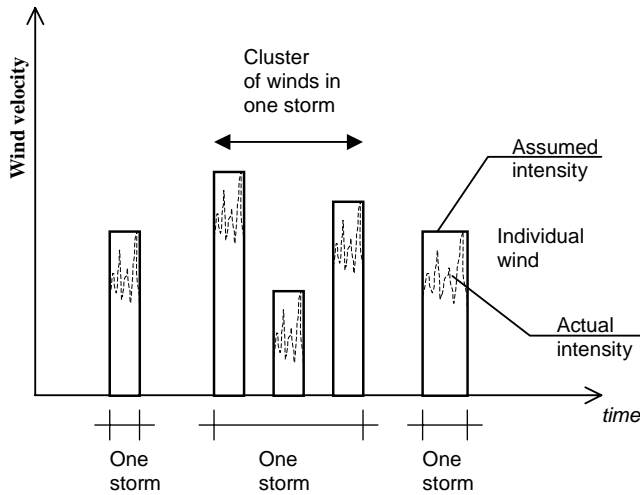


Figure 2.7. Representation of wind events.

lected by Simiu, Changery, and Filliben (1979) and confirmed that wind speeds in the interior are best modeled by a Gumbel distribution. Figure 2.8 gives a curve adapted from Belk and Bennett (1991) that shows the close fit between the Gumbel Type I distribution and the data collected by Simiu, Changery, and Filliben (1979) for yearly maximum wind speeds. In subsequent work, Simiu, Heckert, and Whalen argued that regular wind speeds in interior regions are best modeled as reverse Weibull distributions (Simiu and Heckert, 1995; Whalen and Simiu, 1998). However, describing the reverse Weibull distribution requires three statistical parameters. These three parameters are the mean, the standard deviation, and a cut-off threshold value that describes the maximum tail length of the distribution. Simiu and Heckert (1995) argue that “it is difficult to provide reliable quantitative estimates of the tail length parameters” because of the fluctuations in the available estimates of the cut-off threshold values. Hence, because it is difficult to use the reverse Weibull and until the data on the threshold value are made available, in this study a Gumbel distribution is used to model the wind speeds. The Gumbel assumption is

compatible with the work conducted on the calibration of the ASCE design load criteria. Table 2.7 provides the statistical data for the wind speed of typical U.S. sites as assembled by Ellingwood et al. (1980) based on the work of Simiu, Changery, and Filliben (1979). This data will be used in this study to perform the reliability analysis of bridges subjected to wind loads and the combination of winds and other extreme events.

In addition to the wind speed, Ellingwood et al. (1980), following Simiu, Changery, and Filliben (1979), suggest that the statistical uncertainties caused by the limitations in the number of data points used to find the statistics of the wind speed should be included during the reliability analysis. Ellingwood et al. (1980) found that the statistical uncertainties would produce a COV on the order of 7.5% in the projection of the results to the large period of time. The statistical uncertainties are modeled through the variable  $\lambda_v$  of Equation 2.21.  $\lambda_v$  has a mean equal to 1.0 and a COV equal to 7.5% and follows a normal distribution.

The emphasis of this study is on regular windstorms in interior regions of United States excluding the effect of hurricanes and tornados because of the lack of sufficient data on the effects of these strong winds on typical bridge configurations.

#### 2.4.4 Scour

The HEC-18 design equation for local scour around bridge piers is a function of the flow depth, the pier nose shape, the angle of attack of the flow, the streambed conditions, the soil material size, the diameter of the pier, and the Froude number. The equation that is intended to predict the depth of maximum scour for design purposes is as follows:

$$y_{\max} = 2y_0 K_1 K_2 K_3 K_4 \left(\frac{D}{y_0}\right)^{0.65} F_0^{0.43} \quad (2.22)$$

where

- $y_{\max}$  = the maximum depth of scour;
- $y_0$  = the depth of flow just upstream of the bridge pier excluding local scour;

TABLE 2.7 Wind load data in mph based on Ellingwood et al. (1980)

Site	Annual Maximum		50-Year Maximum	
	Mean Annual Velocity (mph)	COV Annual Velocity	Mean 50-Year Wind Velocity (mph)	COV 50-Year Wind Velocity
Baltimore, MD	55.9	0.12	76.9	0.09
Detroit, MI	48.9	0.14	69.8	0.10
St. Louis, MO	47.4	0.16	70.0	0.11
Austin, TX	45.1	0.12	61.9	0.09
Tucson, AZ	51.4	0.17	77.6	0.11
Rochester, NY	53.5	0.10	69.3	0.08
Sacramento, CA	46.0	0.22	77.4	0.13

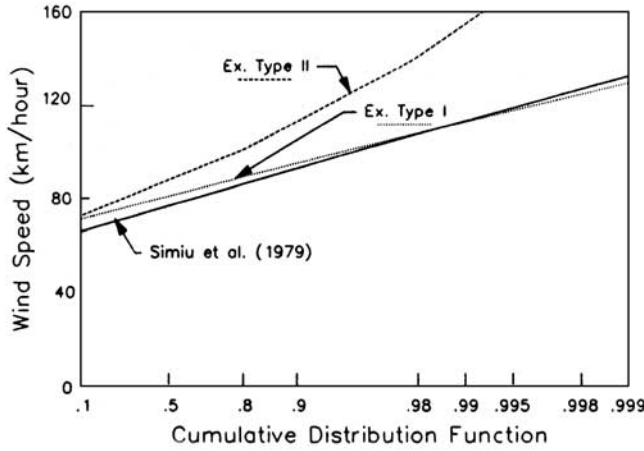


Figure 2.8. Comparison of cumulative probability distribution fit (after Belk and Bennett, 1991).

$K_1, K_2, K_3,$  and  $K_4$  = coefficients that account for the nose shape of the pier, the angle between the direction of the flow and the direction of the pier, the streambed conditions, and the bed material size;

$D$  = the pier diameter; and

$F_0$  = Froude number, which is defined as

$$F_0 = \frac{V}{(gy_0)^{0.5}} \quad (2.23)$$

where  $V$  is the mean flow velocity at the pier, and  $g$  is the acceleration due to gravity.

The flow depth,  $y_0$ , and flow velocity,  $V$ , are related to the flow discharge rate,  $Q$ , at a given point in time and the shape of the channel represented by the cross sectional area of the stream,  $A_0$ . This relationship is given by

$$Q = A_0 V. \quad (2.24)$$

For a rectangular cross section with a constant width,  $b$ , and flow depth,  $y_0$ , the relationship becomes

$$Q = by_0 V. \quad (2.25)$$

The relationship between the flow velocity,  $V$ , and the hydraulic radius that is related to the flow depth,  $y_0$ , can be expressed using Manning's equation:

$$V = \frac{\Phi_0}{n} R_H^{2/3} S_0^{1/2} \quad (2.26)$$

where

$n$  = Manning roughness coefficient,

$R_H$  = the hydraulic radius,

$S_0$  = the slope of the bed stream, and

$\Phi_0$  = a unit adjustment parameter equal to 1.486 when using U.S. units (ft and sec).

For SI units,  $\Phi_0$  equals 1.0. For a rectangular channel of width  $b$ , the hydraulic radius,  $R_H$ , can be calculated by

$$R_H = \frac{by_0}{b + 2y_0}. \quad (2.27)$$

Thus, the relationship between the flow rate  $Q$  and the flow depth  $y$  is given from the equation

$$Q = by_0 \frac{\Phi_0}{n} \left( \frac{by_0}{b + 2y_0} \right)^{2/3} S_0^{1/2}. \quad (2.28)$$

Typical values for Manning's roughness coefficient,  $n$ , vary from 0.025 to 0.035 for earth (respectively for good condition and for weeds and stones). It is noted that estimating the appropriate Manning roughness coefficient is associated with a high level of uncertainty. Researchers at Hydraulic Engineering Center (1986) determined that the roughness coefficient,  $n$ , follows a lognormal distribution with a COV ranging from 20% to 35% (with an average value of 28%). Therefore, in this report,  $n$  is taken as a random variable with a bias equal to 1.0 compared with the recommended tabulated values and a COV equal to 28%. It is also assumed that the slope  $S$  is known and, thus, the uncertainties in  $V$  are primarily due to the uncertainties in estimating  $n$ .

Different researchers and organizations have used different probability distribution types to model the discharge rate,  $Q$ . Extreme Type I distributions, lognormal distributions, and logPearson distributions are most commonly used. By studying several probability plots, the maximum yearly discharge rates for different rivers were found to follow a lognormal distribution. An example of the fit on lognormal probability paper is presented in Figure 2.9 for the Schohaire Creek. Data from five different rivers are also summarized in Table 2.8. The raw data that generated the statistics shown in Table 2.8 were collected from the USGS website. Knowing the probability distribution for the yearly discharge rate, the maximum 75-year flood discharge has a cumulative probability distribution,  $F_{Q75}(x)$ , related to the probability distribution of the 1-year maximum discharge by

$$F_{Q75}(x) = F_Q(x)^{75}. \quad (2.29)$$

Equation 2.29 assumes independence between the floods observed in different years. This assumption is consistent with current methods for predicting maximum floods.

The estimation of the mean and standard deviation of the 75-year maximum discharge rate ( $Q_{75}$ ) for each river, as shown in Table 2.8, is associated with some level of uncertainty. This level of uncertainty depends on the number of samples available to calculate the means and standard deviations. The

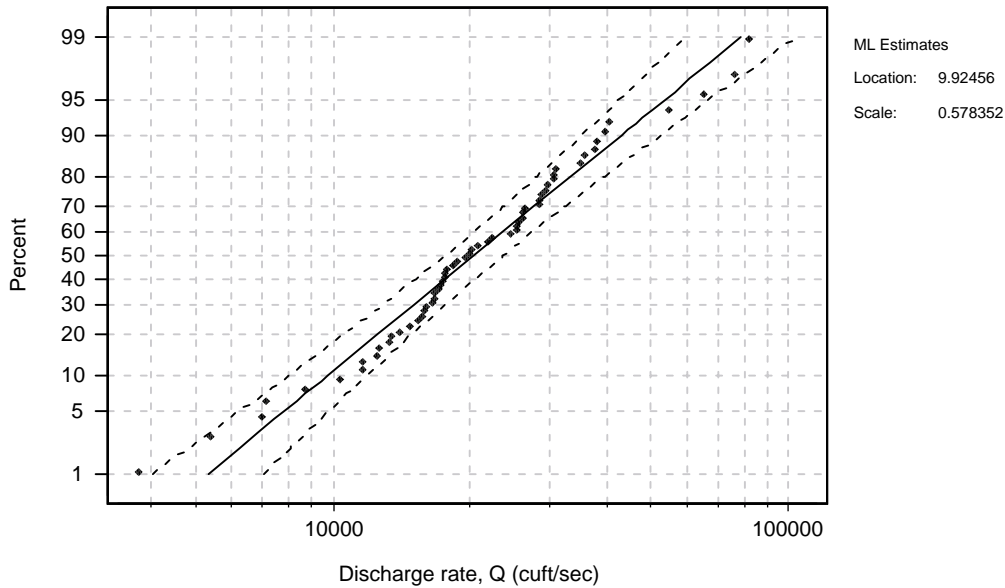


Figure 2.9. Representation of discharge rate for Schohaire Creek on lognormal probability plot.

analysis of the data provided in the USGS website for the five rivers analyzed in this report show that the mean values provided in Table 2.8 are within a 95% confidence level. For this reason, a modeling variable  $\lambda_Q$  is used in this report to express the variability in the prediction of  $Q$ . This modeling variable is thus assumed to follow a normal (Gaussian) distribution and to have a bias of 1.0 and a COV of 5%.

The HEC-18 approach has been extensively used for practical design considerations although the HEC-18 empirical model provides conservative estimates of scour depths and is known to have the following five limitations:

1. The HEC-18 equation is based on model scale experiments in sand. In a recent evaluation against full-scale observations from 56 bridge sites, HEC-18 has been found to vastly over-predict the scour depth (Landers and Mueller, 1996). A comparison of the HEC-18 equation and the measured depths are illustrated in Figure 2.10, which is adapted from Landers and Mueller (1996).
2. Once a flood begins, it takes a certain period of time for the full extent of erosion to take effect. Thus, if the flood is of a short duration, the maximum scour depth may not be reached before the flood recedes. On the other hand, prior floods may have caused partial erosions accelerating the attainment of the maximum scour depth. HEC-18 does not predict the length of time required for the maximum scour depth to be reached and assumes that the maximum depth is always reached independent of the flood duration and the level of scour incurred by prior floods.
3. The HEC-18 model does not distinguish between live-bed scour and clear-water scour in terms of the time required to reach equilibrium scour depth and the differences in the expected magnitudes of scour depths for these different phenomena (Richardson and Davis, 1995).
4. HEC-18 was developed based on experimental data obtained for sand materials. Some work is in progress to study the applicability of HEC-18 for both sand and

TABLE 2.8 Probability models for five rivers

River	Log Q	$S_{\log Q}$	$D_n^*$	Average 75-year $Q, Q_{75}$ (ft <sup>3</sup> /sec)	COV of $Q_{75}$
Schohaire	9.925	0.578	0.067	85,000	29%
Mohawk	9.832	0.243	0.068	34,000	12%
Sandusky	9.631	0.372	0.086	38,000	18%
Cuyahoga	9.108	0.328	0.065	20,000	16%
Rocky River	9.012	0.378	0.049	21,000	19%

\* $D_n$  is the K-S maximum difference between the measured cumulative probability and expected probability value. More than 60 data points were available for each of the five rivers. The  $D_n$  values obtained indicate that the lognormal distribution is acceptable for a significant level  $\alpha = 20\%$ .

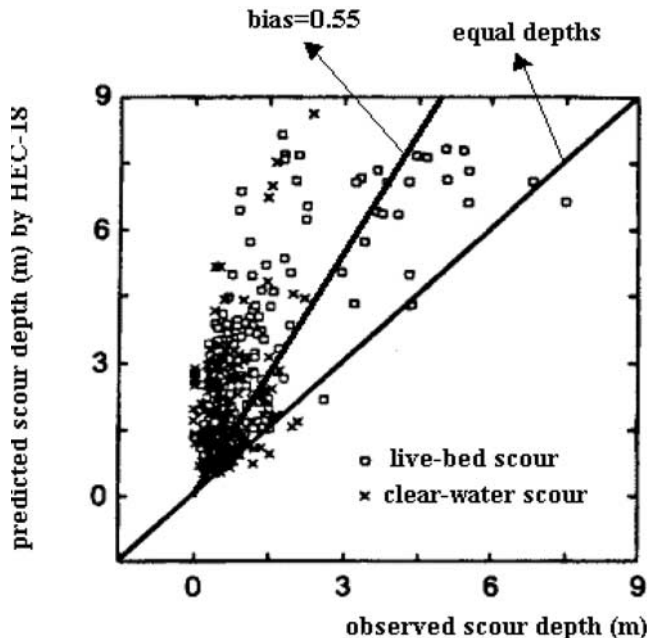


Figure 2.10. Comparison of HEC-18 predictions to observed scour depths (based on Landers and Mueller, 1996, Figure 2).

clay streambed materials because it is well known that these materials behave differently (Briaud et al. 1999).

5. The usual assumption is that scour is deepest near the peak of a flood but may be hardly visible after floodwaters recede and scour holes refill with sediment. However, there are no known methods to model how long it takes a river to backfill the scour hole. Refill can occur only under live-bed conditions and depends on the type and size of the transported bed material (sand or clay). Even when refill occurs, it will take a considerable length of time for the refill material to sufficiently consolidate and restore the pier foundation to its initial strength capacity. Although such information is not precisely available, a number of bridge engineers have suggested that periods of 2 to 3 months are reasonable for sandy materials with longer periods required for clays.

Based on the observations made above, a possible reliability model for the reliability analysis of a bridge pier under the effect of scour is proposed based on the work of Johnson as presented in Appendix B. This model is based on the observation that Equation 2.22 gives a safe value for the depth of scour. The average ratio of the observed scour depth compared with the HEC-18 predicted depth was found by Johnson (1995) to be about 0.55 (bias value is 0.55). Also, the ratio of the true scour value over the predicted value has a COV of 52%. This ratio is represented by a scour modeling variable,  $\lambda_{sc}$ , that is assumed to follow a normal distribution. Thus, according to Johnson (see Appendix B), the true scour value can be represented by an equation of the form

$$y_{max} = 2\lambda_{sc}y_0K_1K_2K_3K_4\left(\frac{D}{y_0}\right)^{0.65}F_0^{0.43}. \quad (2.30)$$

It should be noted that Johnson (1995) also recommends that the factor  $K_3$  representing the effect of streambed condition be treated as a random variable with a bias equal to 1.0 and a COV equal to 5% to account for the possible variability of the streambed between floods. Table 2.9 summarizes the input data for the random variables appropriate for use with Equation 2.30. As indicated above,  $Q$  is a time-dependent variable while the remaining random variables are time-independent. Equation 2.30 assumes that the statistical properties of the modeling variable,  $\lambda_{sc}$ , are constant for all floods and rivers. However, a review of the Landers and Mueller (1996) data plotted in Figure 2.10 has revealed that this is not necessarily the case. For this reason, an alternate model has been developed in Appendix I and is described in the next paragraph.

Equation 2.30 provides a reliability model that is compatible with the models proposed by researchers for the live load, earthquake, and wind events. However, a careful review of the data depicted in Figure 2.10 shows that for low scour depths,  $\lambda_{sc}$  appears higher than the average value of 0.55 and for high scour depths,  $\lambda_{sc}$  appears to be lower. For this reason, an alternate reliability model is proposed based on the regression analysis of the data published by Landers and

TABLE 2.9 Input data for reliability analysis for scour alone

Variable	Mean Value	COV	Distribution Type	Reference
Discharge rate, $Q$	from Table 2.8	from Table 2.8	Lognormal	Based on USGS website
Modeling variable for $Q$ , $\lambda_Q$	1.0	5%	Normal	Based on USGS website
Modeling variable, $\lambda_{sc}$	0.55	52%	Normal	Johnson (1995)
Manning roughness, $n$	0.025	28%	Lognormal	Hydraulic Engineering Center (1986)
Bed condition factor, $K_3$	1.1	5%	Normal	Johnson (1995)
Residual error, $\epsilon$	0.0	Standard deviation = 0.406	Normal	Appendix I

Mueller (1996). Based on the regression fit as described in Appendix I, the observed scour depths around rounded bridge piers founded on non-cohesive soils may be modeled by an equation of the form

$$\ln y_{\max} = -2.0757 + 0.6285 \ln D + 0.4822 \ln y_0 + 0.6055 \ln V + \varepsilon \quad (2.31)$$

where

- $D$  = the pier diameter,
- $y_0$  = the flow depth,
- $V$  = the flow velocity, and
- $\varepsilon$  = the residual error.

As explained above,  $D$  is a deterministic variable because the pier diameter can be accurately known even before the actual construction of the pier.  $y_0$  and  $V$  are random variables that depend on Manning's roughness coefficient,  $n$ , and the 75-year maximum discharge rate, which are random variables having the properties listed in Table 2.9. Based on the analysis of the residuals affected in Appendix I,  $\varepsilon$  may be considered to follow a normal distribution with mean equal to zero and a standard deviation equal to 0.406.

Finally and as mentioned above, it is noted that under live bed conditions, the local scour hole is normally assumed to refill as the scour-causing flood recedes. However, the available literature does not provide precise information on how long it normally takes for the foundation to regain its original strength. This is believed to depend on the type of material being deposited by live-bed streams. For example, fine sands may tend to regain their strengths within a short period of time (perhaps 2 to 3 months). On the other hand, cohesive materials such as clays may take much longer to consolidate and regain their original strengths. As a compromise, the calculations performed in this study will assume that it takes about 6 months ( $1/2$  year) for a foundation to regain its original strength. It is further assumed that the scour depth produced by the maximum yearly flood will remain at its maximum value for this half-year period. This assumption will also indirectly account for the effects of smaller floods within that period of time. The proposed model will also assume that the scour depth will be reached instantaneously as the flood occurs and that the flooding period is always long enough for the maximum scour depth to be reached.

#### 2.4.5 Vessel Collision Forces

Considerable effort was spent on studying vessel collision forces during the development of AASHTO's *Guide Specifications and Commentary for Vessel Collision Design of Highway Bridges* (1991). The AASHTO guide uses a reliability formulation following the recommendations made by several International Association for Bridge and Structural Engineers (IABSE) workshops and symposia. An IABSE

Working Group assembled a state-of-the-art report summarizing the findings of an international group of researchers (Larsen, 1993). The latter document gives an overview of the background information that led to the development of the AASHTO guide specifications. The guide gives an example outlining the application of the guide's Method II, which gives a probability-based analysis procedure for determining the design forces caused by ship impacts with bridges. In addition, Whitney et al. (1996) describe the application of the AASHTO vessel collision model for barge traffic over the Ohio River. The model used in this study to perform the reliability analysis of bridge piers subjected to vessel collisions is based on the guide's Method II and follows the example described by Whitney et al. (1996). The calculations performed for this report are for barge collision forces such as those that may occur at the piers of bridges spanning rivers with heavy barge traffic. Bridges spanning waterways with big ship traffic are normally unique structures that should be studied on an individual basis.

Based on the AASHTO guide method, the design barge collision force can be represented by an empirically derived equation as a function of the barge bow damage depth. The design force equation takes the form

$$P_B = 60a_B \quad \text{for } a_B < 0.1\text{m},$$

and

$$P_B = 6 + 1.6a_B \quad \text{for } a_B \geq 0.1\text{m} \quad (2.32)$$

where  $P_B$  is the nominal design force in MN (meganewtons), and  $a_B$  is the barge bow damage depth.

According to the AASHTO guide specifications, the barge bow depth is calculated from the kinetic energy of the moving barge. Because barges in large rivers travel in flotillas, the kinetic energy that should be used in calculating the collision force should account for the masses of all the barges in a column of the flotilla when head-on collisions are considered. Hence, the kinetic energy  $KE$  is calculated as

$$KE = \frac{C_H W V^2}{2 \times 9.81} \quad (2.33)$$

where

- $W$  = the weight of a flotilla column,
- $V$  = the speed of the flotilla at impact,
- 9.81 = the acceleration due to gravity in  $\text{m/s}^2$ , and
- $C_H$  = a hydrodynamic coefficient that accounts for the effect of the surrounding water upon the moving vessel.

As an example, Whitney et al. (1996) suggest that the value  $C_H = 1.05$  is appropriate for the Ohio River because of the rel-



atively large underkeel clearance and accelerations in the direction of the ship length (i.e., there are no large lateral motions as those associated with barge berthing). The barge damage depth,  $a_B$ , is given as

$$a_B = \frac{[\sqrt{1.00 + 0.13KE} - 1] \times 3.1}{R_B} \quad (2.34)$$

where  $R_B$  is the correction factor for barge width given as  $R_B = B_B/10.68$  where  $B_B$  is the barge width in meters (or  $R_B = B_B/35$  in feet for U.S. units). The correction factor is meant to account for the difference between the width of the barge tested to empirically obtain the barge damage depth equation and the barge width of the impacting vessel.

The kinetic energy of Equation 2.33 must be calculated based on the speed at impact that must account for the speed of the flotilla relative to the river and the river flow speed. When the main piers of a bridge are adjacent to the vessel transit path, the transit speed is used for the relative speed of impact. Otherwise, AASHTO gives an empirical equation that describes how the speed varies from the travel speed to the river flow speed as a function of the distance between the transit path and the pier location. For example, Whitney et al. (1996) found that the flotilla speed in the Ohio River may reach up to 3.13 m/sec (10.3 ft/sec). Given that the river speed is on the average 1.86 m/sec (6.1 ft/sec), the speed at impact will be equal to 4.99 m/sec (16.4 ft/sec).

*Modeling Factor*

Equation 2.32 for the nominal impact force was developed based on experimental data of individual barge collisions with lock entrance structures and bridge piers. These studies included dynamic loading with a pendulum hammer, static loading on barge models, and numerical computations. However, the tests were conducted for single barges at low velocities and not multibarge flotillas traveling at high velocities. Whitney et al. (1996) report that the actual crushing depths as observed from accidents on the Ohio River were much lower than those calculated from the results of the AASHTO equations. This may be due to the significant energy loss that occurs among the barges of the flotilla because of friction and crushing. To correct for the differences between the calculated damage and the observed damage, the AASHTO guide uses a modeling variable,  $x$ . Thus, the actual impact force is given as

$$P = xP_B \quad (2.35)$$

where  $x$  is the modeling variable, and  $P_B$  is the predicted value of the impact force that is given by Equation 2.32.

The random variable,  $x$ , gives the ratio of the actual impact force  $P$  to the nominal impact force  $P_B$ . A probability density

and a cumulative distribution function are given to describe  $x$ , as shown in Figure 2.11 (which is adapted from Figure C4.8.3.4-2 of the AASHTO guide [1991]). For a given value of barge weights in a flotilla column,  $W$ ,  $P_B$  is calculated from Equations 2.32 through 2.34. The probability that  $P$  is greater than a certain fraction of  $P_B$  is obtained from Figure 2.11(b). Figure 2.11 shows that  $P_B$  gives a very conservative estimate of the impact force. For example, Figure 2.11(b) shows that the probability that  $P$  is greater than  $0.1P_B$  (or  $x = P/P_B = 0.1$ ) is only 0.1 (or 10%). The probability that  $P$  is greater than  $0.5P_B$  (or  $P/P_B = 0.5$ ) is 0.0556 (or 5.56%). The probability that  $P$  is greater than  $P_B$  ( $P/P_B = 1$ ) is zero. The AASHTO guide states that the results illustrated in Figure 2.11 were obtained from the work of Cowiconsult (1987) for ship collisions. The same curve was assumed by Whitney et al. (1996) to be valid for collisions of barge flotillas.

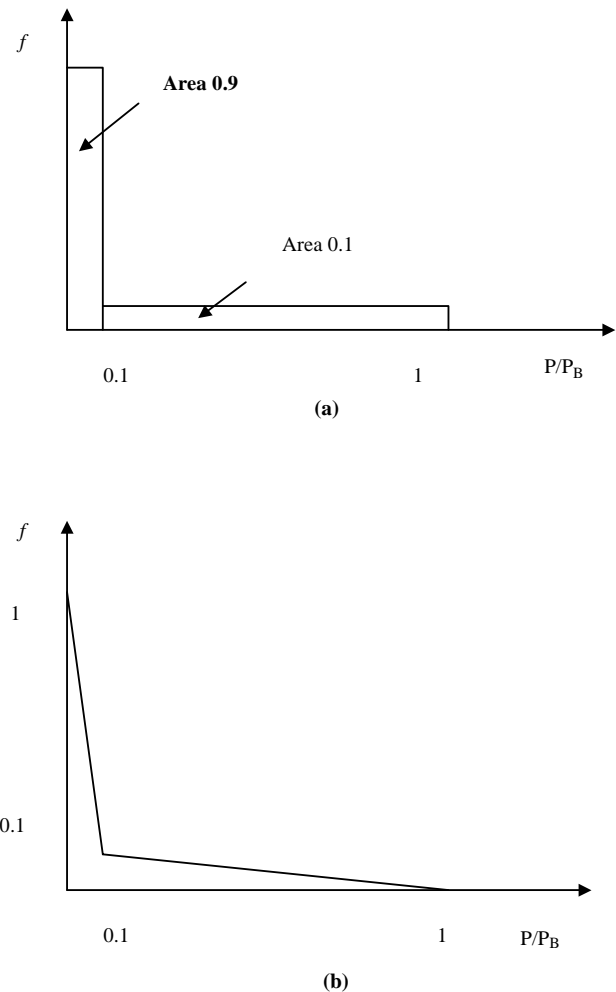


Figure 2.11. Distribution function for vessel collision force modeling variable: (a) probability density function for relative magnitude of the collision force,  $x$ ; (b) distribution function for  $x = P/P_B$  exceeding a given level.

### Rate of Collisions

Equation 2.35 above gives the force at impact given that a barge column with a known weight and speed has collided with a bridge pier. However, because not all flotillas are expected to collide, the reliability calculations must account for the number of collisions expected during the design life of the bridge structure. Although the AASHTO guide specifications develop the design criteria in terms of annual risk, to be consistent with the AASHTO LRFD requirements, bridges should be designed to satisfy a minimum level of reliability for a 75-year design life.

As presented in the AASHTO guide specifications and the IABSE report, the annual failure rate caused by vessel collisions,  $AF$ , can be expressed as

$$AF = \sum_i N_i PA_i \sum_k PG_{i,k} PC_{i,k} \quad (2.36)$$

where

- $N_i$  = the number of vessels (or flotillas) of type  $i$  that cross the waterway under the bridge in 1 year;
- $PA_i$  = the probability of vessel aberrancy (of straying away from normal navigation channel) for vessels of type  $i$ ;
- $PG_{i,k}$  = the geometric probability of collision of ship type  $i$  with bridge element  $k$  (this gives the probability of having a collision with bridge member  $k$ , given that an aberrancy occurred in ship or a flotilla of type  $i$ ); and
- $PC_{i,k}$  = the probability that the bridge will collapse given that a vessel of type  $i$  has collided with member  $k$  of the bridge.

Equation 2.36 leads to the yearly rate of collisions for each vessel (or flotilla) of type  $i$  into a particular bridge element,  $k$ , as

$$v_i = N_i PA_i PG_i. \quad (2.37)$$

Below is a description on the method proposed by the AASHTO guide to calculate the probability of aberrancy and the geometric probability. Using the rate of collisions and the frequency distribution of vessel (or flotilla types), the probability distribution of the force  $P_b$  of Equation 2.32 can be calculated as explained further below.

#### Probability of Aberrancy, $PA_i$

The probability of aberrancy (sometimes referred to as the causation probability) is a measure of the risk of a vessel losing control as a result of pilot error, adverse environmental conditions, or mechanical failure. The AASHTO guide states that the evaluation of accident statistics indicates that human error (causing 60% to 85% of the aberrancy cases) and envi-

ronmental conditions form the primary reasons for accidents. The environmental causes include poor visibility, strong currents, winds, channel alignment, and so forth. The IABSE report (Larsen, 1993) states that statistical data in major waterways show that the probability of vessel aberrancy varies from about 0.5 to 7 in 10,000 passages. Worldwide, the average is about 0.5 in 10,000 passages. Because such data are particularly hard to obtain for new bridge sites, the AASHTO guide proposes an empirical equation based on historical accident data. The AASHTO equation (Equation 4.8.3.2-1 in the AASHTO guide [1991]) accounts for the following factors: (1) the geometry of the navigation channel and the location of the bridge in the channel (turns and bends); (2) the current direction and speed; (3) the crosscurrents; and (4) vessel traffic density. The equation is given as

$$PA = BR_a(R_B)(RC)(R_{XC})(R_D) \quad (2.38)$$

where

- $PA$  = probability of aberrancy;
- $BR_a$  = aberrancy base rate =  $0.6 \times 10^{-4}$  for ships or  $1.2 \times 10^{-4}$  for barges;
- $R_B$  = correction factor for bridge location = 1.0 for straight paths regions (varies as function of angle  $\theta$  for vessel paths with turns and bends);
- $R_C$  = correction factor for current acting parallel to vessel path;
- $R_{XC}$  = correction factor for crosscurrents acting perpendicular to vessel transit path; and
- $R_D$  = correction factor for vessel traffic density depending on the frequency of vessels meeting, passing, or overtaking each other in the immediate vicinity of the bridge.

For example, the actual data collected by Whitney et al. (1996) for barge collisions in the Ohio River shows that the rate of aberrancy has an average value of  $5.29 \times 10^{-4}$ , which is higher than the  $1.20 \times 10^{-4}$  AASHTO value. They also found that the rate of aberrancy was equal to  $13.78 \times 10^{-4}$  for the Tennessee River,  $18.11 \times 10^{-4}$  for the Cumberland River,  $3.14 \times 10^{-4}$  for the Green River, and  $1.2 \times 10^{-4}$  for the Kentucky River. The IABSE report (Larsen 1993) indicates that the probability of collision to bridge piers increases by a factor of 3 when the wind speeds are in the range of 40 to 50 km/h (25 to 30 mph) as compared with the aberrancy rates when the wind speed are 20 to 30 km/h (12 to 19 mph).

#### Geometric Probability, $PG_i$

The geometric probability is defined as the probability of a vessel hitting the bridge pier given that the vessel has lost control. This probability is a function of many parameters, including the geometry of the waterway, the location of bridge piers, the characteristics of the vessel, and so forth. The AASHTO

guide specification developed an empirical approach for finding the geometric probability. The AASHTO approach is based on the following three assumptions:

1. The lateral position of a vessel in the waterway follows a normal distribution with a mean value centered on the required path line (centerline of navigation route).
2. The standard deviation of this lateral position distribution is equal to the overall length of vessel designated as *LOA*. In the case of flotillas, Whitney et al. (1996) recommend using the total length of the flotilla (i.e., barge length times number of barges in a column).
3. The geometric probability is calculated from the normal distribution depending on the location of the pier relative to the centerline of the navigation route, the width and orientation of the pier, and the width of the vessel. For flotillas, the total width of the flotilla should be used.

The method to calculate the geometric probability,  $PG$ , is illustrated in Figure 2.12, which is adopted from the AASHTO guide and the IABSE report. The use of a standard deviation equal to *LOA* was justified based on accident data to reflect the influence of the size of the colliding ship.

*Probability Distribution of the Predicted Impact Force,  $P_B$*

The force  $P_B$  of Equation 2.32 depends on the type of impacting vessel (or flotilla), including the weight of the vessel, its length, and other geometric features. Given the statistical data on the types of vessels (or flotillas) and their properties, the probability distribution of the predicted impacting force  $P_B$  can be assembled. The data on the type of vessels and their weights can be gathered from agencies that track the traffic in U.S. waterways such as the U.S. Army Corps of Engineers (USACE), which has provided data on barge traffic in

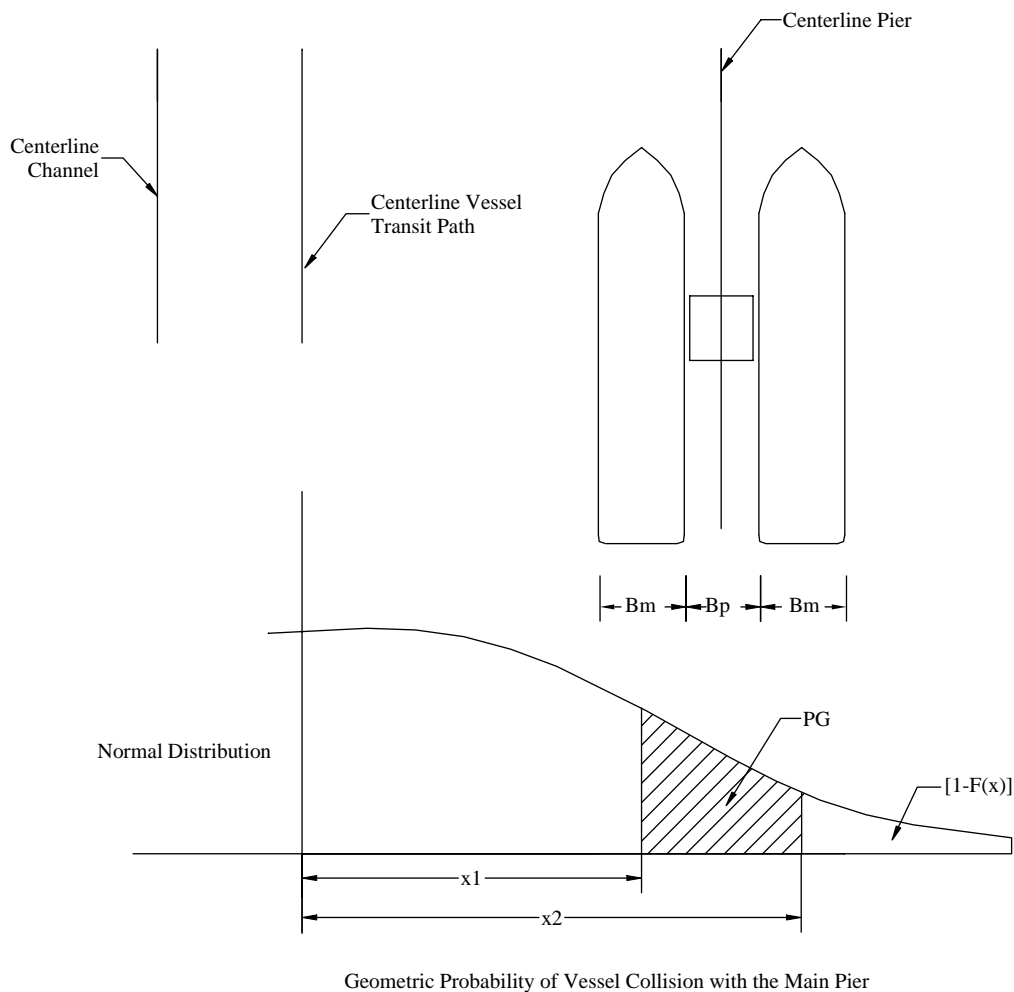


Figure 2.12. Model for geometric probability of vessel collision with main bridge pier [based on the AASHTO guide (1991) and the IABSE report (Larsen, 1993)].

the Mississippi River near Memphis, Tennessee. Figure 2.13 shows the yearly probability distribution function for the impacting force calculated for the Mississippi River based on the USACE’s data. More details explaining how the distribution function was assembled are provided in Appendix D.

The AASHTO guide specifies that when a vessel collides with a bridge pier, the impact force,  $P_B$ , obtained from Equation 2.32, will be applied as a concentrated force at the high water level. Several possible modes of failure may result because of the application of the force,  $P_B$ . The most likely failure modes include shear failure of the pier at the point of impact, moment failure of the pier or the foundation, and soil failure in the pier foundation.

In summary, the model used in this report to study the reliability of a bridge pier subjected to vessel collisions is based on the model proposed by Whitney et al. (1996), which follows the AASHTO model (1991). The process followed consists of the following steps and assumptions:

- The geometric probability,  $PG_i$ , of a flotilla type  $i$  colliding with the bridge pier depends on the flotilla overall length,  $LOA_i$ , as described in Figure 2.12. Each flotilla of type  $i$  may have a different length depending on the number of barges in each column and the length of each barge. To simplify the problem, it is herein assumed that the number of barges in a column of a flotilla is equal to the average number of barges as reported by Whitney et al. (1996).
- The expected number of collisions of flotillas of type  $i$  with the pier is equal to  $N_i PA_i PG_i$  where  $N_i$  is the number of flotillas of type  $i$  crossing the site,  $PA_i$  is the probability

of aberrancy of flotilla type  $i$ , and  $PG_i$  is the geometric probability of collision of flotilla type  $i$ .

- The nominal force applied on the pier if a flotilla of type  $i$  collides with the bridge pier is calculated from Equation 2.31 if the total weight of the flotilla and the width of the impacting barge are known. Each flotilla of type  $i$  may have a different total weight depending on the number of barges in the flotilla and the weight of each barge. Whitney et al. (1996) use the weight of one column of barges to find the kinetic energy at impact. The assumption is that the other columns are loosely tied to the impacting column such that at impact, only the barges in one column will contribute to the impact energy. To simplify the problem, it is herein assumed that the weight is equal to the average number of barges in one column times the average weight of the barges that form the flotilla. Average values for number of barges in a column and barge weights are provided by Whitney et al. (1996).
- By assembling the nominal “average” impact force for each flotilla type and the expected number of collisions for each flotilla type, a cumulative distribution of the yearly impact force can be drawn as is shown in Figure 2.13.
- Equation 2.14 can then be used to find the probability distribution for the 75-year bridge design life or other return periods.

Because  $P_B$  is calculated using the average vessel weight for each vessel type, it is herein proposed to account for the probability of having vessels heavier than the average value. This is achieved by including a weight-modeling factor during the reliability calculations. The data provided by

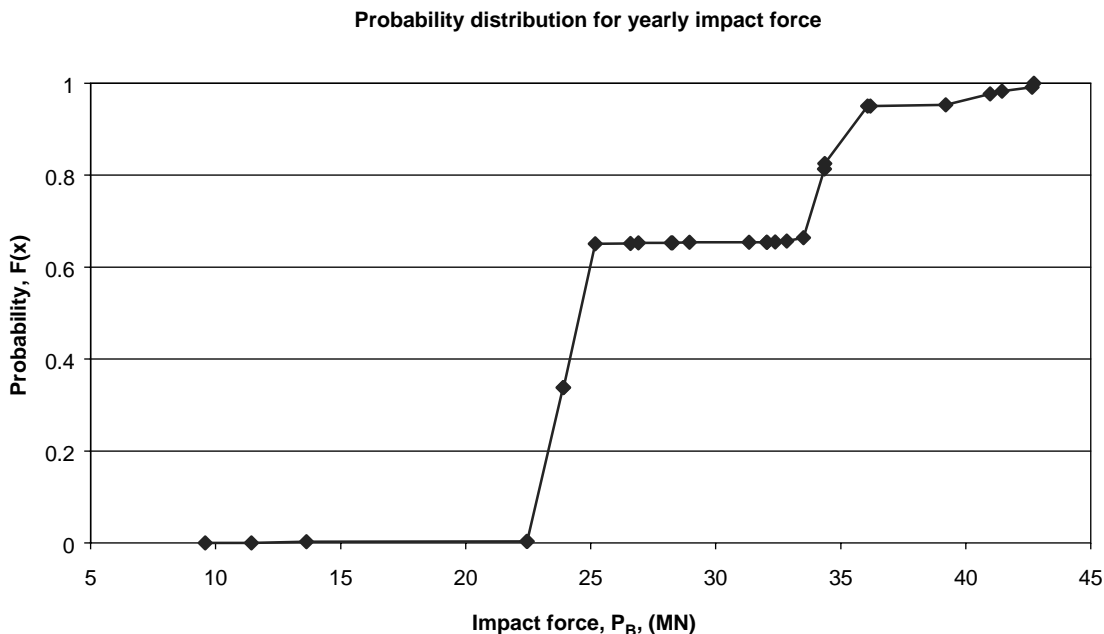


Figure 2.13. Cumulative distribution function for calculated ship collision force,  $P_B$ .

USACE show that the weight-modeling variable has a mean value of 1.0 and a COV of 10%. It is assumed to follow a normal distribution following the suggestion of Whitney et al. (1996). This weight-modeling factor is used to supplement the force-modeling factor  $x$  such that Equation 2.35 is modified to become

$$P = xwP_B. \tag{2.35'}$$

The three random variables— $x$ ,  $w$ , and  $P_B$ —used in modeling the final load effects of impact vessels are summarized in Table 2.10.

### 2.5 RISK ASSESSMENT MODELS FOR LOAD COMBINATIONS

As mentioned in Chapter 1, the Ferry Borges–Castanheta model is used in this report to study the reliability of a bridge system subjected to a combination of load events. In this section, the Ferry Borges–Castanheta model is described for two load processes and is illustrated in Figure 2.14 (Turkstra and Madsen, 1980; Thoft-Christensen and Baker, 1982). The model assumes that each load effect is formed by a sequence of independent load events, each with an equal duration. The service life of the structure is then divided into equal intervals

**TABLE 2.10 Summary of random variables for flotilla collision with bridge pier**

Variable	Symbol	Mean	COV	Distribution Type	Reference
Applied nominal force	$P_B$	from Figure 2.13	from Figure 2.13	from Figure 2.13	Based on AASHTO (1991) and Whitney et al. (1996)
Force-modeling factor	$x$	from Figure 2.11	from Figure 2.11	from Figure 2.11	AASHTO (1991)
Weight-modeling variable	$w$	1.0	10%	Normal	Based on data from USACE

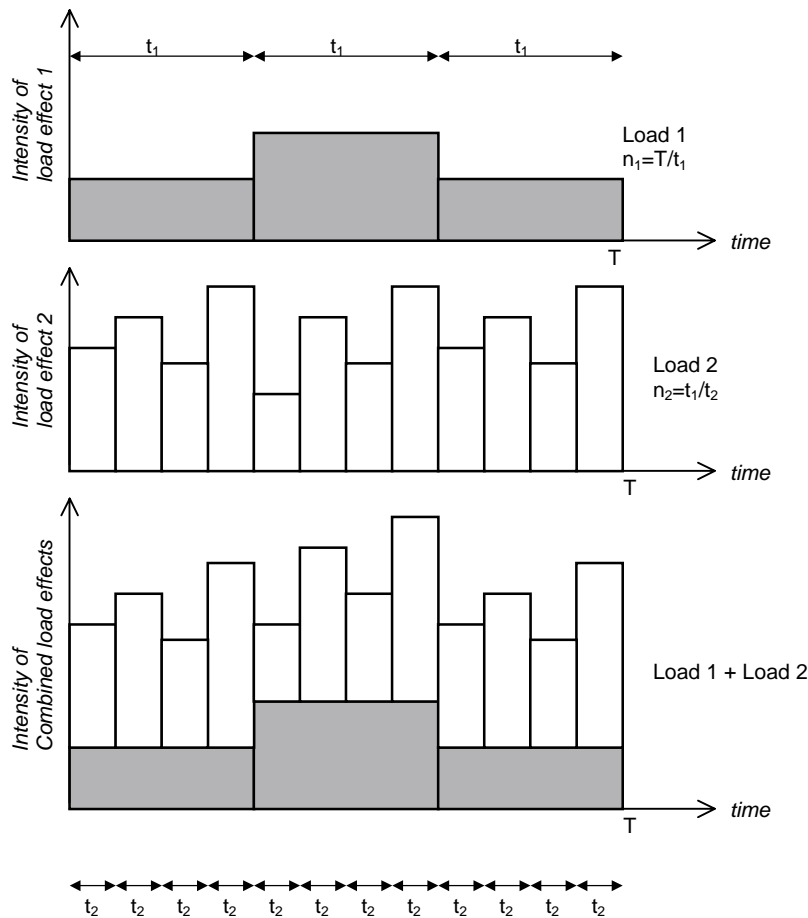


Figure 2.14. Description of Ferry Borges–Castanheta load combination model.

of time, each interval being equal to the time duration of Load 1,  $t_1$ . The probability of Load 1 occurring in an arbitrary time interval can be calculated from the occurrence rate of the load. Simultaneously, the probability distribution of the intensity of Load 1 given that the load has occurred can be calculated from statistical information on load intensities. The probability of Load 2 occurring in the same time interval as Load 1 is calculated from the rate of occurrence of Load 2 and the time duration of Loads 1 and 2. After calculating the probability density for Load 2 given that it has occurred, the probability of the intensity of the combined loads can be easily calculated. The Ferry Borges–Castanheta model can be summarized with reference to Figure 2.14 as follows:

1. The intensity of the effect of Load 1 is a function of time  $t$ , defined as  $x_1$ .
2. The intensity of the effect of Load 2 is a function of time  $t$ , defined as  $x_2$ .
3.  $x_1$  and  $x_2$  vary randomly in function of time as shown in Figure 2.14.
4. Every time Load 1 occurs, it lasts for a fixed time duration equal to  $t_1$ .
5. Every time Load 2 occurs, it lasts for a fixed time duration equal to  $t_2$ .
6. The life span of a bridge structure,  $T$ , is an integer multiple of  $t_1$ .
7.  $t_1$  is an integer multiple of  $t_2$ .
8. Load 1 occurs a total of  $n_1$  times in the life of the bridge ( $T = n_1 \times t_1$ ).
9. Load 2 occurs a total of  $n_2$  times when Load 1 is on ( $t_1 = n_2 \times t_2$ ).
10. Each occurrence of Load 1 is independent from the previous occurrences.
11. Each occurrence of Load 2 is independent from the previous occurrences.
12. Loads 1 and 2 are also independent of each other.
13. The combined load effect is defined as  $X = x_1 + x_2$ .

The load combination problem consists of predicting the maximum value of  $X$ ,  $X_{\max, T}$ , that is likely to occur in the lifetime of the bridge,  $T$ . In this lifetime there will be  $n_1$  independent occurrences of the combined load effect,  $X$ . The maximum value of the  $n_1$  possible outcomes is represented by

$$X_{\max, T} = \max_{n_1}[X] \quad (2.39)$$

The maximum value of  $x_2$  that is likely to occur within a time period  $t_1$  (when Load 1 is on) is defined as  $x_{2 \max, t_1}$ . Since Load 2 occurs  $n_2$  times within the time period  $t_1$ ,  $x_{2 \max, t_1}$  is represented by

$$x_{2 \max, t_1} = \max_{n_2}[x_2] \quad (2.40)$$

$X_{\max, T}$  can then be expressed as

$$X_{\max, T} = \max_{n_1}[x_1 + x_{2 \max, t_1}] \quad (2.41)$$

or

$$X_{\max, T} = \max_{n_1}\left[x_1 + \max_{n_2}[x_2]\right] \quad (2.42)$$

The problem will then reduce to finding the maximum of  $n_2$  occurrences of Load 2, adding the effect of this maximum to the effect of Load 1, then taking the maximum of  $n_1$  occurrences of the combined effect of  $x_1$  and the  $n_2$  maximum of Load 2. This approach assumes that  $x_1$  and  $x_2$  have constant intensities during the duration of one of their occurrences. Notice that  $x_1$  or  $x_2$  could possibly have magnitudes equal to zero. If the intensities of  $x_1$  and  $x_2$  are random variables with known probability functions, then  $X_{\max, T}$  can be calculated as described below.

The cumulative distribution of any load  $Y$  can be represented as  $F_Y(Y^*)$ .  $F_Y(Y^*)$  gives the probability that the variable  $Y$  takes a value less than or equal to  $Y^*$ . Most load combination studies assume that the load intensities are independent from one occurrence to the other. In this case, the cumulative distribution of the maximum of  $m$  events that occur in a time period  $T$  can be calculated from the probability distribution of one event by

$$F_{Y_{\max, m}}(Y^*) = F_Y(Y^*)^m \quad (2.43)$$

where  $m$  is the number of times the load  $Y$  occurs in the time period  $T$ .

Equation 2.43 is obtained by realizing that the probability that the maximum value of  $m$  occurrences of load  $Y$  is less than or equal to  $Y^*$  if the first occurrence is less than or equal to  $Y^*$ , and the second occurrence is less than or equal to  $Y^*$ , and the third occurrence is less than or equal to  $Y^*$ , and so forth. This is repeated  $m$  times, which leads to the exponent  $m$  in the right-hand-side term of Equation 2.43.

The cumulative probability distribution of  $x_{2 \max, t_1}$  is found by plugging the probability distribution of  $x_2$  into the right-hand side of Equation 2.43 with  $m = n_2$ . Then, knowing the distribution of  $x_1$ , combine the distribution of  $x_1$  and  $x_{2 \max, t_1}$  to find the distribution of their sum. Finally, use this latter distribution in the right-hand side of Equation 2.43 with  $Y$  representing the combined effect and  $m = n_1$  to find the probability distribution of  $X_{\max, T}$ . Given the statistics of the resistance and the probability distribution of  $X_{\max, T}$ , which is the maximum load effect in the lifetime of the structure, a Level II reliability program or a Monte Carlo simulation can be used to find the reliability index  $\beta$ . The reliability index will provide a measure of the level of safety of a bridge member under the combined load effect, as was described in Section 2.2.

This approach, which assumes independence between the different load occurrences, has been widely used in many previous efforts on the calibration of the load factors for com-

binned load effects. However, in many practical cases, even when the intensities of the extreme load events are independent, the random effects of these loads on the structure are not independent. For example, although the wind velocities from different windstorms may be considered independent, the maximum moments produced in the piers of bridges as a result of these winds will be functions of modeling variables such as pressure coefficients and other statistical uncertainties that are not independent from storm to storm. In this case, Equations 2.42 and 2.43 have to be modified to account for the correlation between the intensities of all  $m$  possible occurrences. For example, let us assume that the load effect  $x_1$  of Equation 2.42 is the product of a time-dependent random load intensity  $z_1$  and a time-independent analysis variable  $c_1$  where  $c_1$  describes how the load intensity is converted to a load effect. Similarly, the load effect  $x_2$  is the product of a time-dependent random load intensity  $z_2$  and a time-independent analysis variable  $c_2$  that describes how the load intensity is converted to a load effect. In this case, Equation 2.42 can be expanded as

$$X_{\max, T} = \max_{n_1} \left[ c_1 z_1 + \max_{n_2} [c_2 z_2] \right] \quad (2.44)$$

where  $c_1$  and  $c_2$  are time-independent random variables that do not change with  $n_1$  and  $n_2$  while the load intensities  $z_1$  and  $z_2$  are time-dependent variables that increase as the return periods represented by the number of occurrences  $n_1$  and  $n_2$  increase.

The randomness in  $c_1$  and  $c_2$  can be accounted for by using conditional probability functions; that is, Equation 2.43 can be used to determine the distribution function of  $X_{\max, T}$  for pre-set values of the analysis modeling factors  $c_1$  and  $c_2$ , which are assumed to be constant. Then, knowing the probability that  $c_1$  and  $c_2$  are equal to the pre-set values, the final unconditional probability of  $X_{\max, T}$  is obtained by summing together the products of the probability associated with each value of the modeling factor and the outcome of Equation 2.43. This can be represented by the following equation:

$$\begin{aligned} \Pr[X_{\max, T} \leq X^*] &= F_{X_{\max, T}}(X^*) \\ &= \iint F_{X_{\max, T}}(X^* | c_1, c_2) f_{c_1}(C_1) f_{c_2}(C_2) dc_1 dc_2 \end{aligned} \quad (2.45)$$

where  $F_{X_{\max, T}}(X^* | c_1, c_2)$  is the probability function of  $X_{\max, T}$  conditional on particular values of  $c_1$  and  $c_2$  and  $f_{c_1}$  and  $f_{c_2}$  are the probability density functions of the analysis variables  $c_1$  and  $c_2$ .

The model described above based on Figure 2.14 assumes that the return period  $T$  can be exactly divided into  $n_1$  occurrences of the Load 1 where the time duration of each occurrence is  $t_1$  such that  $T = t_1 n_1$ . Modifications on the classical model can be made to describe situations when no loads are on. For example, these can be accounted for by using a cumulative probability distribution function  $F$  with high probability values for  $X = 0$ . Also, if the time duration

of the loads is short, the Ferry Borges–Castanheta model can be represented as shown in Figure 2.15, in which the basic time interval  $t_1$  represents the recurrence interval of Load 1. For example, if a load is known to occur on the average once every year, then  $t_1 = 1$  year is used, and  $n_1$  the number of repetitions in a 75-year return period will be  $n_1 = 75$ . Using the same logic,  $n_2$  becomes the average number of occurrences of Load 2 in the time period,  $t_1$ . For example, if on the average there are 200 wind storms in 1 year, then  $n_2 = 200$  when  $t_1 = 1$  year.

### 2.5.1 Scour as a Special Case

The combination of the effect of scour with the other extreme events does not follow the assumptions of the models described above. This is because scour does not produce a load effect on bridge structures but changes the geometry of the bridge pier so that the effects of the other loads are amplified. This phenomenon is illustrated in Figure 2.16.

For example, let us assume that a bridge pier has a height equal to  $h$ . When the pier is subjected to a lateral force of magnitude  $P$ , the moment at the base of the pier is originally equal to  $Ph$ . The random variable  $P$  could be the force caused by wind pressure or may describe the impact force caused by the collision of a vessel with the pier. If the foundation of the pier has been subjected to a random scour depth equal to  $y_{\text{scour}}$ , then, after the occurrence of scour, the moment at the base of the pier will be equal to

$$M_{\text{scour}} = P(h + y_{\text{scour}}). \quad (2.46)$$

Thus, the combined effect of ship collision (or wind load) and scour is multiplicative, not additive as described above. The probability of failure will then be equal to the probability that  $M_{\text{scour}}$  is greater than the moment capacity of the pier or the moment capacity of the foundation. If the foundation is very deep, then the moment capacity will remain the same as it was before scour. In this case, the moment arm of the load,  $P$ , changes as the point of fixity in the foundation is shifted downward. If the foundation is not deep, the ability of the foundation to resist overturning may decrease because of the occurrence of scour. In this case, the capacity of the foundation will need to be calculated based on the remaining foundation depth and the type of soil. Another mode of failure is the loss of serviceability caused by the lateral deflection of the pier-superstructure system. That is, the foundation may not fail, but the flexibility of the pier-foundation system after scour may produce large deformations in the structure, rendering it unfit for use.

A model to obtain the probability distribution of the maximum scour depth,  $y_{\text{scour}}$ , for different return periods is presented in Section 2.4.4. Section 2.4 also presents models to obtain the probability distribution of the maximum force effect,

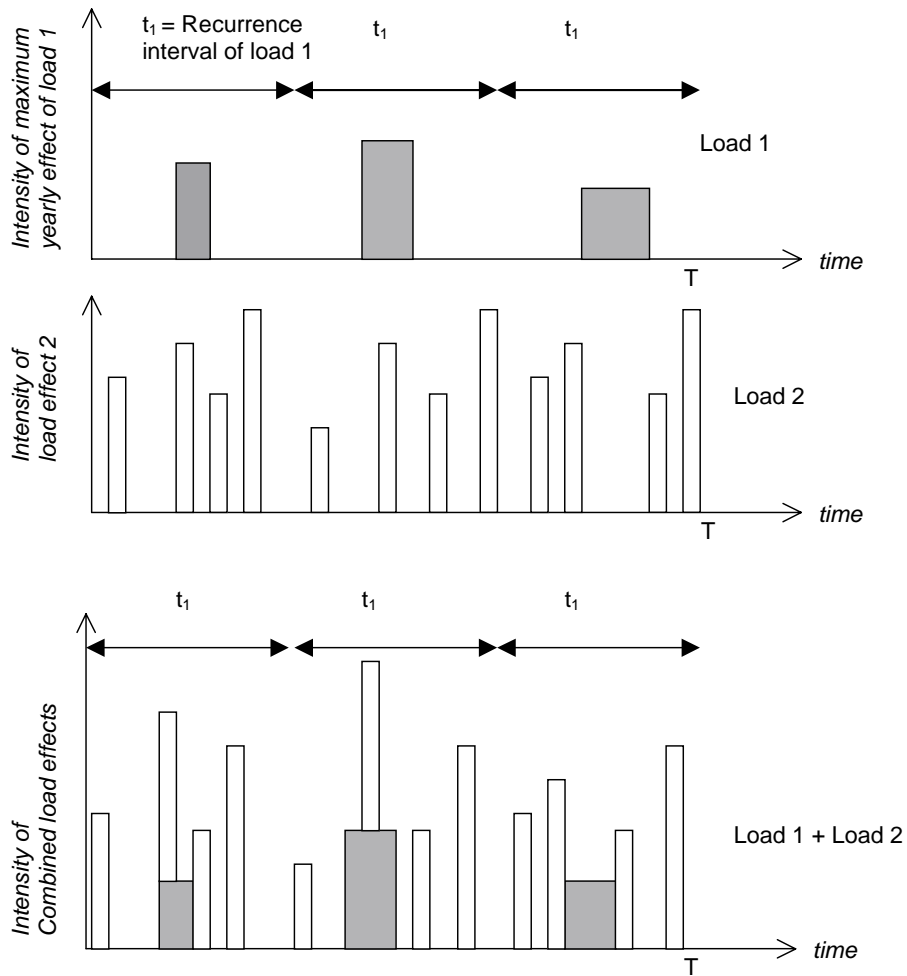


Figure 2.15. Modified Ferry Borges–Castanheta model.

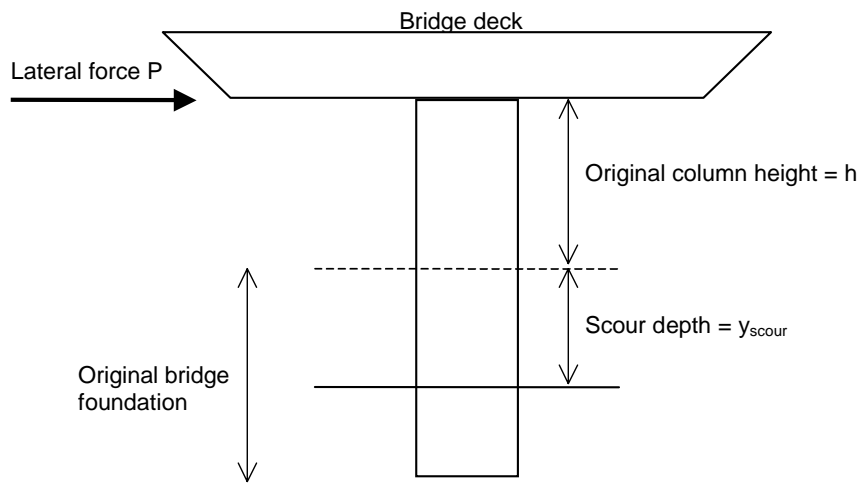


Figure 2.16. Representation of combination of scour and other loads.



$P$ , as a function of the return period for the extreme load events of interest to this study. The maximum moment effect caused by the combination of scour and the other extreme events can then be calculated using the expression for  $M_{\text{scour}}$  as is shown in Equation 2.46.

It is noted that the presence of scour would alter the natural period of the bridge system, rendering it more flexible. The additional flexibility induced by the presence of scour may sometimes reduce the inertial forces produced by dynamic vibrations, such as those caused by earthquakes, rendering the structure less vulnerable to these threats. Hence, the presence of scour may under certain circumstances be beneficial and improve the reliability of the structure. Therefore, it is critical to check the safety of bridges with and without scour to ensure that the worst conditions are accounted for.

## 2.6 CHAPTER CONCLUSIONS

This chapter described the models used in this study to perform the reliability analysis of highway bridges subjected to extreme events and the combination of extreme events. As a first step, the statistical information necessary to perform the reliability analysis has been assembled from the literature and, when possible, as used during previous code development efforts. The modified Ferry Borges–Castanheta model used in this study to perform the reliability analysis for the combination of load events has also been described. Examples illustrating the use of the proposed models are provided in the appendixes. The results are summarized and used to propose a set of load factors for the combination of extreme events, as will be described in Chapter 3.

---